2014

Numerical Uncertainty in Simulation of Room Ventilation

Aaron Alexander Aczel
University of Windsor

Numerical Uncertainty in Simulation of Room Ventilation

by

Aaron Alexander Aczel

A Thesis
Submitted to the Faculty of Graduate Studies
through the Department of Mechanical, Automotive and Materials Engineering
in Partial Fulfillment of the Requirements for
the Degree of Master of Applied Science
at the University of Windsor

Windsor, Ontario, Canada
2014

NUMERICAL UNCERTAINTY IN SIMULATION OF ROOM VENTILATION

By:

Aaron Alexander Aczel

APPROVED BY:

_____

Dr. X. Xu
Department of Civil and Environmental Engineering

_____

Dr. R. Barron
Department of Mechanical, Automotive and Materials Engineering

_____

Dr. G. Rankin, Advisor
Department of Mechanical, Automotive and Materials Engineering

August 21, 2014

DECLARATION OF CO-AUTHORSHIP / PREVIOUS PUBLICATION

I. Co-Authorship Declaration

I hereby declare that this thesis incorporates material that is result of joint research, as follows:

This thesis also incorporates the outcome of a joint research undertaken in collaboration with Dr. Mo Karimi under the supervision of Dr. G.W. Rankin. In all cases, the key ideas, primary contributions, data analysis and interpretation, were performed by the author, and the contribution of co-authors was primarily of an advisory nature.

I am aware of the University of Windsor Senate Policy on Authorship and I certify that I have properly acknowledged the contribution of other researchers to my thesis.

II. Previous Publication

I certify that, with the above qualification, this thesis, and the research to which it refers, is the product of my own work.

This thesis includes one original paper that has been previously published/submitted for publication in a peer reviewed journal, as follows:

Thesis Chapter	Publication title/full citation	Publication status*
Portions of Chapter 3 and Chapter 4	*Aczel, A., Karimi, M. and Rankin, G.W., 2013, "Effect of Boundary Conditions on Room Ventilation Simulation Uncertainty", International Journal of Surface Engineering & Materials Technology, Vol. 3 No. 1, pp 34-38.*	*Published*

I certify that I have obtained a written permission from the copyright owner(s) to include the above published material in my thesis. An image of the written permission is included in Appendix A. I certify that the above material describes work completed during my registration as a graduate student at the University of Windsor.

I declare that, to the best of my knowledge, my thesis does not infringe upon anyone's copyright nor violate any proprietary rights and that any ideas, techniques, quotations, or any other material from the work of other people included in my thesis, published or otherwise, are fully acknowledged in accordance with the standard referencing practices. Furthermore, to the extent that I have included copyrighted material that surpasses the bounds of fair dealing within the meaning of the Canada Copyright Act, I certify that I have obtained a written permission from the copyright owner(s) to include such material(s) in my thesis.

I declare that this is a true copy of my thesis, including any final revisions, as approved by my thesis committee and the Graduate Studies office, and that this thesis has not been submitted for a higher degree to any other University or Institution.

ABSTRACT

Numerical solutions for fluid dynamic problems must be validated using experimental results. Uncertainties of the numerical scheme and in the experimental data as well as the physical input parameter values must be considered. The American Society of Mechanical Engineers published a standard procedure which accounts for these factors. This standard is used here as the basis for a procedure to determine the uncertainty in velocity magnitude values obtained from a numerical simulation of air flow within a small room using a commercial solver. The interior of the room includes occupants, computers, desks, cabinets and ceiling lights. Cold air is supplied to the room through a diffuser on one of the walls while warm air exits through a vent in the ceiling. The relative importance each factor contributes to the overall uncertainty is investigated to demonstrate the technique. Aspects of the standard are investigated and modifications suggested which simplify its application.

DEDICATION

I would like to dedicate this work to my loving wife Alexandra. In all of my work, you provide me the light, guidance and love that I need to get through. I love you. I would also like to thank my supervisor, Dr. Gary Rankin for his time and patience. It has been a long and drawn out journey, but the end is now very near. I would also like to thank my family: parents Tony and Mary Ann, mother-in-law Gabi Smith, brother and sister-in-law Adam and Heather, and finally my younger brother, Aric. All of you have been an inspiration to me and have always been there for me – I thank you and love you all.

ACKNOWLEDGEMENTS

I would like to thank the University of Windsor and specifically the Mechanical, Automotive and Materials Engineering Department for their support. I would also like to thank Dr. Barron and Dr. Xu for providing me with a great, knowledgeable committee. Finally, thank you to the engineers who have always strived for excellence and helped me throughout the writing of this thesis – especially Mo Karimi, Kohei Fukuda and Ali Salih.

TABLE OF CONTENTS

LIST OF TABLES

LIST OF FIGURES

ABBREVIATIONS

ACH	Air changes per hour
AIAA	American Institute of Aeronautics and Astronautics
ASHRAE	American Society of Heating, Refrigerating and Air-Conditioning Engineers
ASME	American Society of Mechanical Engineers
CAD	Computer Aided Design
CFD	Computational Fluid Dynamics
PDE	Partial Differential Equations
FVM	Finite Volume Method
GCI	Grid Convergence Index
GRF	Grid Refinement Factor
HVAC	Heating, Ventilation and Air Conditioning
LES	Large Eddy Simulation
RE	Richardson Extrapolation
RMS	Root Mean Square
RNG	Re-Normalization Group

NOMENCLATURE

a	width used for hydraulic diameter
b	height used for hydraulic diameter
d_h	hydraulic diameter
D	experimental data value
e_a	approximate relative error
e_{ext}	extrapolated relative error
E	experimentally measured value
F_s	factor of safety
f	estimated value
f_t	true value
h	grid spacing value
H	inlet height
N	total number of cells
p	observed order
q	heat flux
$q(p)$	function equation for observed order p
Q_{inlet}	inlet flow rate
r	grid refinement factor
$RNG\ k-epsilon$	re-normalized group k-epsilon turbulence model
s	returned sign of negative or positive
S	numerical solution value
S_j	average of velocity

S_{ji}	baseline value of model output
S_{ji}^{-}	model output at input parameter, shifted in the negative direction from base input
S_{ji}^{+}	model output at input parameter, shifted in the positive direction from base input
T	true (but unknown) value
u_h	ordered discretization error uncertainty
U_H	uncertainty of inlet (diffuser) height
u_i	estimated iteration error uncertainty
u_{input}	overall uncertainty of inputs to the system
u_{num}	numerical uncertainty
u_{total}	total uncertainty
u_{val}	model validation uncertainty
U_{Power}	power uncertainty
$U_{Q_{inlet}}$	inlet flow rate uncertainty
$U_{Voltage}$	voltage uncertainty
U_s	uncertainty of the simulated result
$U_{V_{inlet}}$	inlet velocity uncertainty
U_W	uncertainty of inlet (diffuser) width
$U_{x\%}$	uncertainty estimate with probability x%
V_{inlet}	inlet velocity
ΔV_i	volume of i^{th} cell
W	inlet width
x_i	input values at pole x and height i

Greek Letters

σ	Gaussian distribution range
∂x_i	partial pole location
δ_S	error in simulated values
δ_{model}	error in model values
δ_D	error in experimental values
δ_{num}	error in numerical values
δ_{input}	error in input parameters
ε	difference between mesh results at a given point
φ	numerical solution result at a given point
φ_{ext}	extrapolated value

CHAPTER 1 Introduction

In the developed world, there has been an increased effort to achieve the goal of improving building energy efficiency by minimizing energy usage in heating, ventilating and air-conditioning (HVAC) applications, while maintaining or improving occupant comfort. In order to achieve this goal, building design optimization needs to be considered. It is unrealistic to build numerous experimental facilities to evaluate different methods and arrangements. A more efficient approach is to use computational fluid dynamics (CFD). To encourage this practice and assist designers in its implementation, the American Society of Heating, Refrigerating and Air-Conditioning Engineers (ASHRAE) includes sections on CFD, meshing, boundary conditions, modeling techniques as well as verification, validation and reporting results in its chapter on Indoor Environmental Modeling starting with the 2009 edition of their Fundamentals Handbook [1].

When numerically modeling HVAC problems, however, numerous difficulties arise. Some of these include the proper treatment of natural convection from heated surfaces, flow turbulence and radiation heat transfer as well as the vast differences in length scales of geometry. To understand and evaluate the performance of the simulation results, numerical data validation is critical. This can be accomplished through the completion of experimental studies and comparison with numerical work. Once the techniques have been validated they can be applied to new designs. In order to establish a standard procedure for determining numerical data validation, the American Society of Mechanical Engineers (ASME) has developed a general industry standard specific to CFD and heat transfer problems [2]. This thesis is an investigation of an application of

that procedure to a specific office HVAC problem for which experimental data is available.

1.1 Scope

This thesis is organized in the following manner. Chapter 2 includes a review of pertinent literature regarding topics of importance to this thesis. It begins with a brief historical account of the development of error estimation techniques associated with CFD, and more specifically CFD for office building studies. Finally, the specific objectives of this work are presented along with directions to be taken to accomplish these objectives. This is followed by Chapter 3, which describes the numerical study portion of this work, and gives specific details regarding the geometry of the room, the grid, boundary conditions, model setup, and the numerical experiments completed. Chapter 4 discusses the results of the experimental and total/overall uncertainties, and also gives insight into streamline plots generated around an anomalous point. Chapter 5 includes conclusions drawn from the aforementioned work and recommendations for future work.

CHAPTER 2 Literature Review and Objectives

The focus of this work relates to literature in the following areas: 1) the development of numerical verification and validation techniques and 2) the rise in importance and application of CFD to building ventilation studies along with validation techniques used. The topics are briefly considered independent of one another in the remainder of the chapter. The chapter concludes with specific objectives that have been formulated through the evolution of this work.

2.1 Validation and Uncertainty in Computational Fluid Dynamic Methods

The rise of CFD is associated with the advent of the digital computer which dates back to the late 1960's. According to Freitas [3], the first record of an event which addresses numerical uncertainty is the set of papers edited by S.J. Kline et al. [4]. Another early paper presented on this topic was by Ghia et al. [5] at the 1981 ASME Winter Annual Meeting. In this early work the focus was on trying to correlate CFD results with experimental results and understand the discrepancies between them.

Interest in improving the accuracy of computational methods, as opposed to determining the uncertainty of the numerical solution, predates the modern digital computer. Prior to the availability of computers, calculations were completed manually using mechanical calculators. This was evident in early work conducted by Richardson, which was first published in 1910 [6]. This century old work is considered to be the first documented iterative CFD solution [7]. The work that Richardson conducted is a method for obtaining a higher-order estimate of the final value to be determined as grid spacing approaches zero, from a lower-order discrete value [8]. This method is termed Richardson Extrapolation (RE).

Roache discussed the estimation of errors in CFD in a general way, including such factors as the order of the discretization as well as grid convergence. His most important contribution to this study is the incorporation of Richardson's work in his development of a generalized approach to numerical "uncertainty" estimation associated with the solution grid size. He referred to this as Grid Convergence Index (GCI) [5-7].

Although error estimates and uncertainty estimates are related, they are not equivalent. The difference between them is that error is supposed to provide improvement in the result, whereas uncertainty provides the range surrounding the estimated value, f, where the true value, f_t, exists with a specific probability value [2]. In standard practice, the common uncertainty probability target for both experiments and computations is 95%. This yields the interval of $f \pm U_{95\%}$. This 95% confidence level is compatible with the range of 2σ in a Gaussian distribution; however, the method does not necessarily depend on this or any other type of distribution.

The GCI is estimated by multiplying the absolute value of the generalized RE by a determined factor of safety, F_s. The purpose of this factor of safety is to convert an estimate of error into an uncertainty estimate, with 95% confidence. The value of the factor of safety is somewhat arbitrary and depends upon the number of grid sizes used to determine the estimate.

Roache's use of RE assumes that the true values are based on a power series representation in the grid spacing, h. If the formal order of accuracy of the code is known, two grids are sufficient for determination of the GCI. However, when the order of accuracy is not known, a minimum of three grids is necessary in order to observe convergence and the associated error estimate. One of the advantages of Roache's

technique is that the typical, but difficult to achieve, approach to grid refinement by doubling or halving the grid to reach grid independence is not necessarily required. Prior to calculating the estimated discretization error, iterative convergence is mandatory. Incomplete iteration can be detrimental to the uncertainty estimation, generating false values. In addition, the use of the RE magnifies incomplete iteration errors.

During the 1980's and 1990's considerable effort was put into understanding the verification and validation of computational fluid dynamic simulations to provide guidance in their determination. This initiative includes an array of papers and journals [9-11] along with textbooks on the subject, such as [12]. The most recent and comprehensive document was published by ASME in 2009 [2]. This document provides a general method applicable to various levels of computational modeling (simple lumped parameter models to 1-D steady laminar flows to 3-D unsteady turbulent flows). The procedures followed in the current thesis are based on this document, which includes some terminology such as validation, code verification, solution verification, error and uncertainty which are explained below.

Validation is defined as the determination of the degree to which a model is an accurate representation of the real situation. The objective is to estimate the range within which the simulation modeling error lies. To accomplish this, the simulation solution must be compared with experimental data for defined validation variables under specified conditions. Code verification is a determination of whether the code accurately solves the physical model that is represented by the code. Solution verification is an estimate of the numerical accuracy of a particular calculation. Error is the difference between the

prediction and the true value, while the uncertainty is a parameter which characterizes the dispersion of the predicted values that could reasonably be expected to occur.

The objective is to quantify the degree of accuracy of the simulation of a particular variable to be validated at some validation point for the conditions of the actual experiment. This can be described using Figure 2.1.

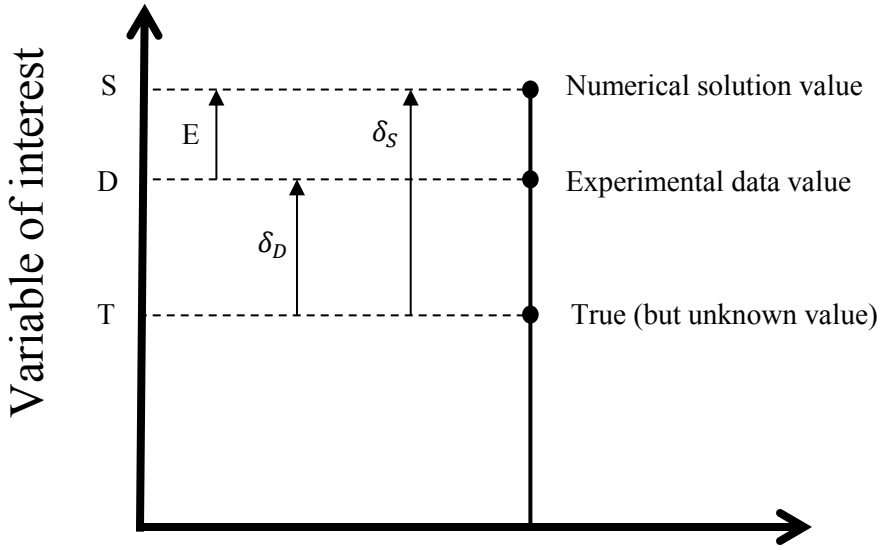

Figure 2.1 Relationship between errors in the variable of interest

The error in the numerical solution, which is the difference between the numerical solution value and the experimentally measured value, *E*, can be seen to be related to the true value, *T*, and the errors in the simulated and experimental values, δ_S and $\delta_{D,}$ as follows:

$$E = S - D = (T + \delta_S) - (T + \delta_D) = \delta_S - \delta_D \tag{2.1}$$

The error in the simulation, δ_S, is assumed to be the sum of the errors due to modeling assumptions and approximations, $\delta_{model,}$ the numerical solution of the

equations, δ_{num} and the errors in the simulation input parameters (geometrical, dynamic and fluid properties), δ_{input} , that is,

$$\delta_S = \delta_{model} + \delta_{num} + \delta_{input} \tag{2.2}$$

It is desired to determine δ_{model} from the other error values and hence

$$\delta_{model} = E - (\delta_{num} + \delta_{input} - \delta_D) \tag{2.3}$$

While the value of *E* is known, the other quantities in the equation are not. The uncertainties of the other quantities, however, can be estimated as u_{num}, u_{input} and u_D.

Also, the uncertainty of the model validation, u_{val}, can be defined as an estimate of the standard deviation of the parent population of the combination of errors $(\delta_{num} + \delta_{input} - \delta_D)$. If they are independent, then

$$u_{val} = \sqrt{u_{num}^2 + u_{input}^2 + u_D^2} \tag{2.4}$$

From the equation above,

$$E - u_{val} < \delta_{model} < E + u_{val} \tag{2.5}$$

Details of how the values required for determining the uncertainty in the validation are calculated and provided as needed throughout the thesis.

2.2 Building Ventilation Studies and CFD

Before the introduction of computational fluid dynamics, ventilation within rooms and buildings was determined using both analytical and empirical methods, some of which are still in use today. Recently, Chen et al. [13] presented an overview of tools used to determine building ventilation performance. He identified the following

classifications; analytical models, empirical models, experimental models (small-scale and full-scale), multi-zone network models, zonal models, and Computational Fluid Dynamics (CFD) models. Analytical models are some of the oldest methods for predicting ventilation performance. This type of method affords easy interpretation as it directly relates to fundamental physical laws and there is little need for computational resources. It is, however, limited to simple geometrical configurations. Empirical models of common flows such as jets and plumes are used to estimate velocities at various places within the occupied spaces caused by inflows through diffusers and other situations. Experimental scale models have been used for determining ventilation flow fields but are generally associated with analysis rather than prediction and full-scale models are often used for mathematical model validation. Multi-zone models involve the solution of the mass, energy and chemical-species conservation equations in zones (or rooms) to determine airflow and contaminant transport between the zones of a building as well as between the building and the outdoors. The models assume still air with a uniform temperature and concentration within the zone and also ignore the momentum effects. Zonal models typically divide a room into less than one thousand three-dimensional cells. The models use mass and energy balance equations to determine air temperature and velocity values which predict the non-uniform distribution in the space. Computational fluid dynamic models use various approaches to solve the partial differential equations (PDE) which represent the velocity, temperature and concentrations fields within the building spaces. Chen investigated the relative popularity of these techniques [14]. The results indicated in Table 2.1 are extracted from his paper. The popularity of CFD is quite evident.

Table 2.1 Percentage of research papers regarding building ventilation studies listed by model type in 2007

Method	Percentage of Papers
Analytical	3
Empirical	2
Experimental	15
Multi-Zone	7
Zonal	3
CFD	70

Early CFD code development focused on the aerospace industry in the 1960s and 1970s, and gradually spread to other industries. Nielsen et al. [15] and Nielsen [16] initiated some of the first work which utilize computers to solve numerical problems associated with building ventilation. The fact that this publication appeared in an ASHRAE journal indicates its acceptance as a valid approach for use in building heating and ventilation applications.

Throughout the years, usage of computational fluid mechanics in predicting building ventilation has steadily increased. This is evident by investigating statistics regarding the number of papers published per year since the early work. To give an idea of the trend, a search was conducted using Compendex with the following keywords appearing in the title, abstract or keywords: computational fluid dynamics, building and ventilation. The results are presented for five year periods in Figure 2 and show the gradual increase in popularity of the approach.

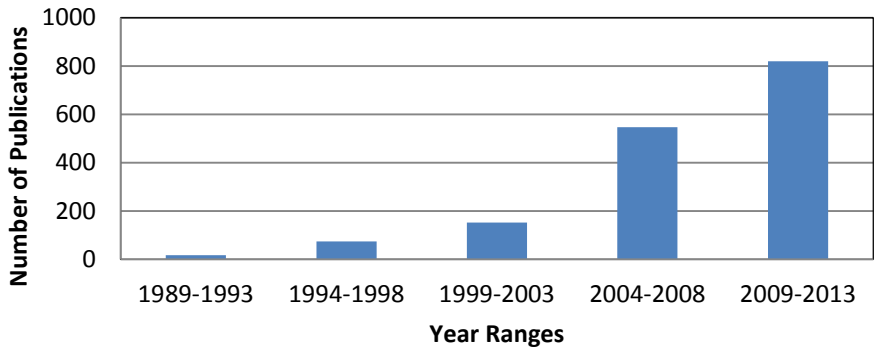

Figure 2.2 Number of CFD building ventilation publications per year ranges

There are many examples of papers within this group that have validated their numerical results using experimental data [15, 17-20]. The numerical approaches include such methods as finite differences and large eddy simulation (LES) techniques.

One of these studies, which included a particularly extensive experimental study, was conducted by Chen et al. [21] as part of an ASHRAE sponsored research project. The experiment involved simulated heat sources from people, office equipment and light fixtures which complicated the room flow patterns through the introduction of natural convection. Details of the room geometrical configuration, the experimental test initial and boundary conditions that were used as well as particulars regarding the measurement equipment used are well documented. A simple numerical method was also included in the report for comparison with the data. Although there was general agreement in the trends between the results, no systematic effort was made to explain the differences between the experimental and numerical results. In view of the above mentioned information, the room configuration and conditions used in this reference was selected to be simulated in this thesis and the uncertainties in the simulation have been evaluated to determine the validity of the solution in comparison with the experimental data.

Most of the computational fluid dynamic papers cited in the literature include some form of grid independence study and validation scheme. No paper concerning CFD in buildings, however, could be found which applied the techniques outlined in the ASME Standard.

2.3 Objectives

The following are the objectives of this study:

- To investigate the application of the numerical uncertainty estimation technique found in the ASME V&V 20-2009 Standard for the case of a building ventilation situation which in turn requires:
    - Development of a numerical finite volume model to solve the problem.
    - Determination of grid and time independence suitable for efficient calculations.
    - Identification of the information from the original experiments necessary for the current uncertainty estimates, and
    - Collection of data obtained from experiments conducted using the numerical model in order to determine the various components required for uncertainty estimates.
- To evaluate the relative contribution of the various factors affecting the values of the uncertainties considered.
- To investigate features of the flow field within the room and identify those features which are responsible for certain anomalous behaviour associated with the determination of uncertainty values.

- To identify and discuss any difficulties in the use of the standard procedure along with how they can be overcome.

CHAPTER 3 Methodology of the Numerical Study

The numerical study conducted to demonstrate the ASME uncertainty methodology is a simulation of the experimental facility used by Chen et al. [21]. His work was conducted as an ASHRAE research project, and included the construction of an experimental room. The experimental room is essentially a box with dimensions of 3.65 m x 5.16 m x 2.43 m, and was built in an environmental test facility at the Massachusetts Institute of Technology in the late 1990's.

The test facility is a well-insulated enclosure with a forced air ventilation inlet, exhaust outlet at the centre of the ceiling, a double-glazed window on the wall opposite to the inlet, two computers, two occupants, six overhead lights, and office furniture: two tables and two cabinets. The occupants are simulated using rectangular boxes containing light bulbs as heat sources. A list of all of the interior objects and their respective dimensions is given in Appendix B along with specific coordinate information to locate them in the room.

The numerical geometry of the room is created using the Computer Aided Design (CAD) software Catia V5 and a wireframe representation of the room and its contents shown in Figure 3.1. The room's contents are composed of the following items: inlet (1), outlet (2), lights (3), desks (4), cabinets (5), occupants (6), computers (7) and a window. The coordinate system is shown in the upper right portion of Figure 3.1. The lower corner of the room at the back and on the right of the diagram is identified to be the origin. The three-dimensional coordinates of the items are all specified from the origin to the closest point on the item. All of these dimensions are presented in Appendix C.

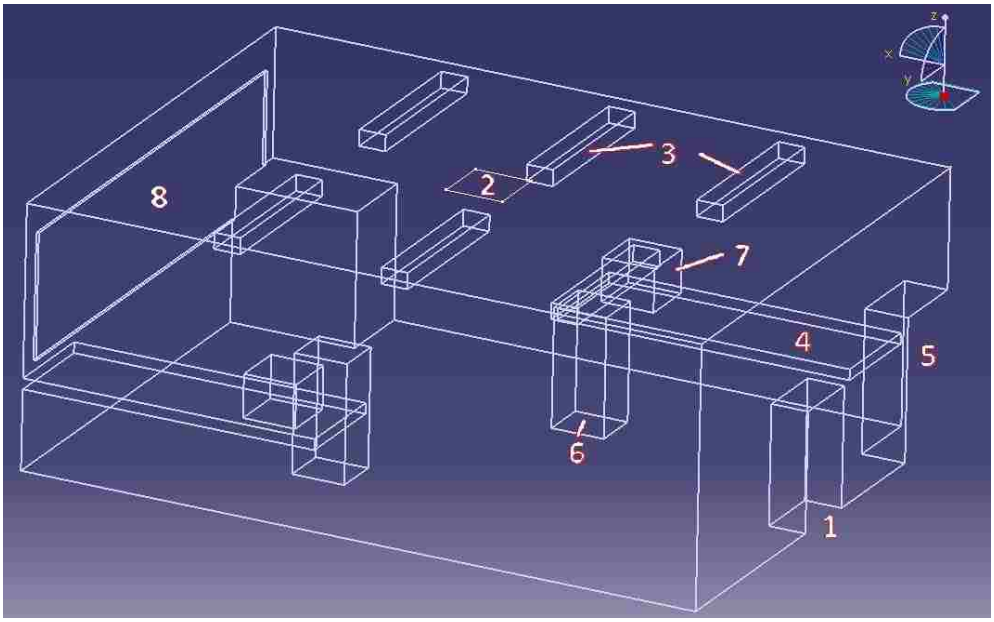

Figure 3.1 Wireframe geometry of office room

The room also has various pieces of instrumentation located throughout the domain to collect velocity data. Hot-sphere anemometers are used to measure air velocity. This equipment is rated for a measurement range of 0.05 to 5 m/s, with a repeatability of 2% (or 0.01 m/s), and cannot reliably measure velocity when it reaches levels below 0.1 m/s. The probes are 0.003 m in diameter. Moveable poles are placed throughout the room in nine different locations as shown in Figure 3.2 to collect air velocity data. Each pole is configured with six hot-sphere anemometers at different heights which are the same height on every pole.

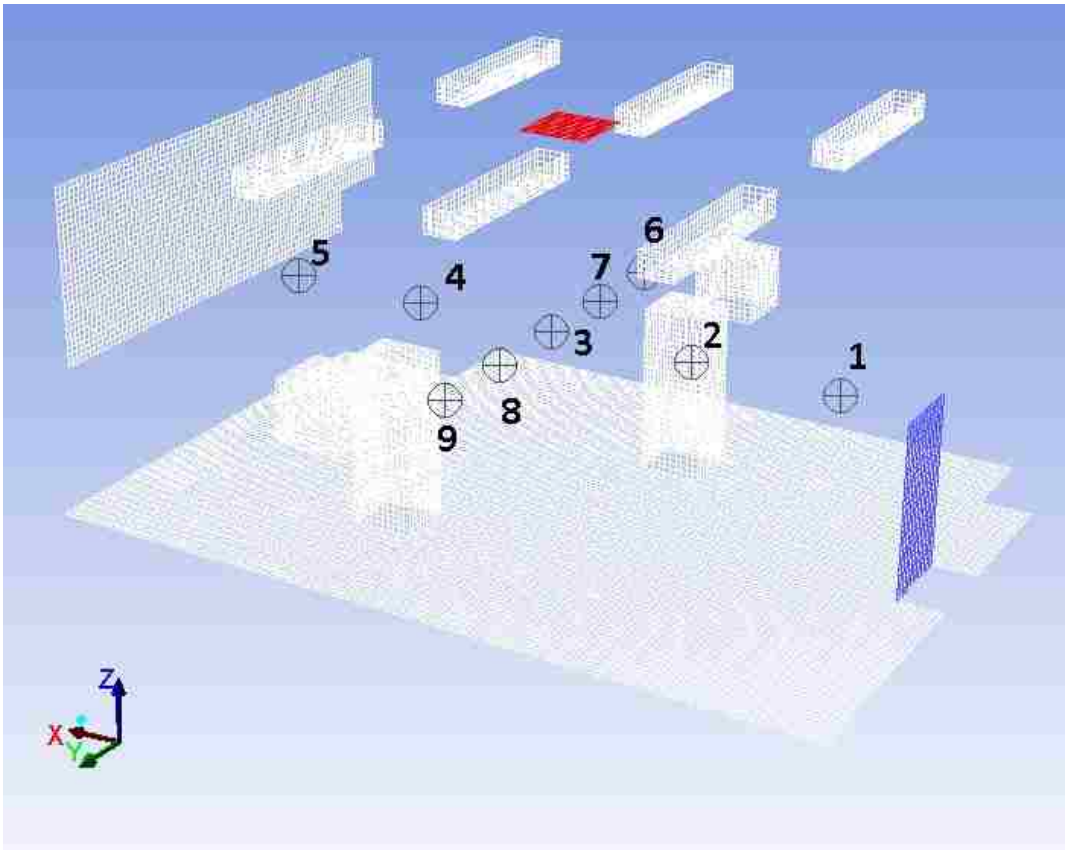

Figure 3.2 Measurement pole locations in office room

The data is measured in the steady state by allowing the test room to stabilize thermal and fluid conditions for half a day before recording any data.

3.1 Numerical Mesh and Nominal Boundary Conditions

The grid generated to model the flow field is constructed using the ANSYS meshing software Gambit. All of the grids employ a structured, hexahedral form. The four meshes constructed through this methodology have the following element count: 229,766; 716,538; 1,834,309; and 5,576,928. These grids are required in order to select the grid used in the remainder of the uncertainty study as well as in the determination of the Grid Convergence Index (GCI). The meshes and their associated maximum skewness factors are presented in Table 3.1. Skewness is a measure of the difference between the

cell and a perfect cube with equivalent volume and is determined here using the Normalized Equiangular Skewness definition [22]. Since this mesh utilizes hexahedral elements, the ideal case would be for all cells to be cubes (which is not the case). The maximum cell skewness in a 3-D simulation should not exceed 0.9, which all meshes remain well under this value [22]. If the value exceeds 0.9, then the mesh will have to be modified because accuracy will be affected and there could be convergence issues. As the mesh gets finer, the skewness value decreases, which is expected, since the cells within a mesh become less distorted as they become close to a cube [22].

Table 3.1 Grids and skewness factors

Grid	Element Count	Maximum Skewness
N1	5576928	0.182710
N2	1834309	0.197133
N3	716538	0.292164
N4	229766	0.380430

All grids are developed in a similar manner, and maintain a consistent cell size variation throughout the geometry. All areas within the domain are treated the same and no clustering or focus was placed on any specific area of the grids.

The nominal boundary condition values were determined using information based on Yuan et al. [23], and all other supplemental information was taken from Chen et al. [21]. The inlet flow rate is specified as air changes per hour (ACH). Along with the inlet width and height dimensions from Appendix C, this produces an average inlet velocity of 0.0864 m/s. No turbulence characteristic information is specified at the inlet diffuser. As it is intended to use the $RNG\ k-epsilon$ turbulence model it is necessary to specify an inlet turbulence intensity level, along with a hydraulic diameter, d_h[24]. The inlet

diffuser is specified to be perforated and Zhang et al. [25] have reported that for perforated plates and grills, typical inlet turbulence intensity values are, respectively, 8 and 10 percent. Since the literature only specifies perforated, but does not specify if it is a plate, an average value (9%) is taken. The hydraulic diameter is defined as [26]:

$$d_h \equiv 4\frac{cross-sectional\ area\ duct}{wetted\ perimeter\ of\ duct} \tag{3.1}$$

In the case of a rectangular cross-section, equation (3.1) simplifies to:

$$d_h = 2\frac{ab}{a+b} \tag{3.2}$$

where a is the width, and b is the height which, in this case, gives a value of 0.717 m.

The outlet from the room is considered to be a pressure outlet, and is assumed to be at a value of 0 kPa gauge pressure. All of the desks and cabinets are considered to be adiabatic. The vertical walls, ceiling and floor have specified temperatures, as provided by Chen et al. [21]. The temperature values were as given in the experimental setup at various locations on each surface. For the purpose of this work, those values are averaged over the entire surface, as denoted in Table 3.2. The experiments, carried out by Chen et al. [21], made use of two different case studies for the test room: cooling and heating. Only the cooling case data are used in this work.

Table 3.2 Average wall temperature values used in CFD

Surface	Location	Experimental Temperature (°C) Measurement	Average Temperature (°C) for CFD
South Wall	1	23.31	25.05
	2	24.41	
	3	25.73	
	4	26.02	
	5	25.78	
East Wall	1	24.18	26.15
	2	24.64	
	3	27.22	
	4	28.13	
	5	26.57	
North Wall	1	25.05	25.50
	2	25.95	
West Wall	1	25.37	25.37
Floor	1	21.54	23.72
	2	23.34	
	3	23.90	
	4	24.24	
	5	24.72	
	6	23.80	
	7	24.11	
	8	24.01	
	9	23.86	
Ceiling	1	25.16	25.55
	2	25.40	
	3	26.19	
	4	25.87	
	5	26.13	
	6	24.90	
	7	24.95	
	8	25.50	
	9	25.89	

The occupants are simulated using rectangular boxes, and contain three 25 W light bulbs to generate a heat source equivalent to that typically released by a human.

Computer 1 has a heat dissipation of 108.8 W and computer 2 has a heat dissipation rate of 173.4 W and they are situated on the desks. The lights are of the general fluorescent type with 2 lamps (34 W) per unit. The heat sources are all modeled as heat fluxes on the box surfaces determined using the following equation:

$$q = \frac{heat\ source\ (W)}{surface\ area\ (m^2)} \tag{3.3}$$

3.2 Numerical Method of Solution

The finite volume method (FVM) as implemented in the ANSYS Fluent 13.0 [22] computational software package is used in this work. Unsteady flow is considered to allow the presence of oscillations as observed in similar studies [27]. The unsteady mass conservation equation, along with the x, y and z momentum equations and the energy equation are solved in order to determine the values of temperature, pressure and the three components of velocity. The turbulence model selected is the $RNG\ k-epsilon$. The reason for this choice is that standard k-epsilon is based on the assumption of high Reynolds number flow, whereas the RNG version is valid for both high and low Reynolds number flows, such as in the office area considered here [24]. This also involves the use of separate transport equations which lead to length scales and turbulent viscosities computed independent of one another.

The air in the office room is assumed to be incompressible and have a density of 1.225 kg/m^3. In order to account for natural convection, the Boussinesq approximation is used. This model treats density as constant in all of the equations, except in the momentum equation's buoyancy term. It induces fast convergence in the solver, and is quite accurate providing changes in the actual density are negligible [22]. The

gravitational force is taken into account and given the constant value of 9.81 m/s^2 in the downward vertical direction.

The discretization scheme is second-order upwind which increases the numerical accuracy compared to first-order schemes. For flows of this type, it is suggested for pressure-based solvers, that PRESTO! be used as the spatial discretization method [22]. This method also works well for iterative time-advancement problems with small time steps. PISO was used for pressure-velocity coupling along with second-order implicit method for increased accuracy of the transient formulation. By means of a time independence study, using all of the same inputs and grid N3 the differences between a time step of 0.5 seconds and 1.0 second is considered to be negligible and a time step of 0.5 seconds was selected for use in the remainder of the calculations in this study. Finally, the computation time difference between 0.5 seconds and 1.0 second was minimal, so this further solidified the selection of 0.5 seconds.

3.3 Numerical Experiments and Determination of Uncertainty Contributions

This section begins with the initial calculations that are conducted to determine when the steady state solution has been reached. These conditions are used in the remainder of the numerical experiments. The rest of this chapter describes the procedures followed to obtain the data necessary for determining estimates of the contribution to the uncertainty in the final result due to the input parameters, u_{input} , grid convergence, u_{num} , and experimental results, u_D.

3.3.1 Determining Steady State Values

As mentioned previously, the unsteady forms of the equations are solved to obtain the final steady state solution. This requires the adoption of a technique for determining

when the steady state condition has been reached. The absolute residual values should not be used for this purpose as they are global values. Instead, the velocity magnitude values at 54 points scattered throughout the room are continuously monitored until a repeated pattern is observed. These 54 points correspond to 9 different pole locations, used in the earlier experimental work. These results are presented and discussed in Chapter 4.

3.3.2 Procedure for Obtaining the Uncertainty Due to the Inputs, u_{input}

The procedure for determining the overall uncertainty in a calculated result described in the ASME Standard includes an estimation of the uncertainty due to the inputs to the model, or u_{input}. In the current study, the experimentally determined values of the boundary conditions for the numerical solution are considered likely to have the greatest effect on this value. The boundary conditions chosen for consideration in this study are: inlet velocity, inlet temperature, heat sources, wall temperatures, turbulence intensity, and outlet pressure. The method of estimating the uncertainties in each of these quantities is described below.

In the experimental setup, the inlet flow rate is stated to be 4 ACH. Normally when a number is specified, the implied error can be taken to be ±0.5 of the least significant digit, or ±0.5 ACH in this case. Using the room dimensions to calculate volume, the inlet flow rate, Q_{inlet}, becomes 0.0509 m^3/s. Using the ACH uncertainty, the uncertainty of the inlet flow rate, $U_{Q_{inlet}}$ is determined to be ±0.00636 m^3/s.

Since the diffuser width and height are 0.53 m and 1.11 m respectively, the inlet velocity is 0.0864 m/s. If it is assumed that the uncertainty in the width and height are each taken to be ±0.005 m, the uncertainty of the inlet velocity is determined as follows:

$$U_{V_{inlet}} = V_{inlet} * \sqrt{\left(\frac{U_{Q_{inlet}}}{Q_{inlet}}\right)^2 + \left(\frac{U_w}{W}\right)^2 + \left(\frac{U_H}{H}\right)^2} \quad (3.4)$$

$$= 0.011 \text{ m/s}$$

For the heat sources, which include the overhead lights, computers, and mocked up version of the occupants, the uncertainty is determined to be ±10% of the device wattage. This estimate is based on North American Standards. In the United States and Canada [28], the nominal voltage at the source is specified to be 120V with an allowable range of ±5%, giving the range of 114V to 126V (RMS). Assuming that the device resistance is constant:

$$\frac{U_{Power}}{Power} = 2 * \frac{U_{Voltage}}{Voltage} \quad (3.5)$$

The above equation (3.5) gives the uncertainty of power equal to ±10% of the device wattage. This not only applies to the overhead lights and computers, but also to the experimental approximation of occupants, which consist of three 25W light bulbs per occupant.

Considering the wall temperatures and inlet temperature, the experimental setup in Chen et al. [21] states that the temperature data taken from these locations is subject to the limitations of the equipment, which has an uncertainty of ±0.44°C.

The wall temperature values specified were average measured values at a number of points on each wall. The uncertainty is based on the standard deviation of temperature values used along with the Student's t value (95% level).

It was also suggested to consider the turbulence intensity of the inlet diffuser. Zhang et al. [25], provides information regarding diffusers of the grill and perforated-panel type. Since the diffuser on hand is listed as perforated, but does not specify further,

a nominal value between both cases is used. The perforated panel has a turbulence intensity of 8%, while the grill has an intensity of 10%. The nominal value between this is 9%, so the value used in the parametric study is 9%±1%. The hydraulic diameter was calculated based on equation (3.1), and uses the same length uncertainty of ±0.005m as used in determining the inlet velocity.

Finally, the outlet pressure as well as the atmospheric conditions of the room air are assumed to have an extremely small influence on the results. It is also assumed that there is no effect of uncertainty in the room size or any other geometrical location of the objects included within the rooms. Thus, both of these types are considered to have negligible impact on the results of the final solution and parametric study. In order to account for all of these parameters, Table 3.3 provides a summary of the above information.

Table 3.3: Summary of input parameters

Parameter	Basis of Estimation	Parameter Value	Uncertainty
Inlet Velocity	Experimental ACH (4 ±0.5) and the height (0.53 ±0.005 m) and width (1.11 ±0.005 m) of the diffuser	0.086 m/s	±0.01 m/s
Inlet Temperature	Experimental value specified	15.0°C	±0.44 °C
Inlet Turbulence Intensity	Average of data for two possible types of inlet diffuser and difference is uncertainty	9%	±1%
Inlet Hydraulic Diameter	Correlation with hydraulic diameter and its estimate based on inlet sizes	0.717 m	±0.005 m
Wall Temperatures	Average measured values at a number of points on each wall – uncertainty based on standard deviation of the temperature values used along with the Student's t value (95% level)	North Wall - 25.5°C East Wall - 26.1°C West Wall - 25.4°C South Wall - 25.0°C	±0.86 °C
Heat Sources (lights, computers and occupants)	Simulated using incandescent lights. Resistance assumed constant and voltage varied by ±5%	Occupant - 75 W Computer 1 - 108 W Computer 2 - 174 W Light - 34 W	±10% of wattage value

The numerical method described in Section 3.2 is used to determine the overall uncertainty based off the model inputs, u_{input}. If the inputs are considered to be truly independent, the uncertainties may be estimated as follows:

$$u_{input_j} = \pm\sqrt{\sum_{i=1}^{N}\left(\frac{\partial S_j}{\partial x_i}u_{x_i}\right)^2} \approx \sqrt{\sum_{i=1}^{N}\left(\frac{S_{ji}^{+}-S_{ji}^{-}}{2}\right)^2} \quad \text{P(\%)} \tag{3.6}$$

where x_i values are the inputs and the S_{ji}^{-} and S_{ji}^{+} values are the solution values at x_i decreased and increased by their uncertainty, respectively. In order to numerically determine the velocity uncertainties using the aforementioned equation, S_j is considered to be the steady state value of velocity at one of the 6 locations on pole 4. As per Table 3.3, there are 6 input values with 6 values of u_{ji} at each location (36 for all 6 locations). It is required to determine the S_{ji}^{-} and S_{ji}^{+} values for each of the 6 input parameters resulting in 12 numerical runs. Finally, the baseline case, S_{ji}, must also be included resulting in a total of 13 runs that must be completed in order to assess all input parameter uncertainty.

3.3.3 Procedure for Obtaining the Uncertainty in the Numerical Solution, u_{num}

The ASME Standard requires that the uncertainty in the numerical solution of the equations, δ_{num}, be estimated. This consists of three parts, round-off error, iterative convergence and discretization error. Round-off error is a consequence of the finite precision of the computer used and assumed to be negligible. Iterative convergence, in the global sense, is often determined by requiring that the value of the residuals of the solved equations decrease by at least two to three orders of magnitude over the entire domain. For time-dependent simulations, local iterative convergence of the final steady state value, u_i , is determined by collecting data points at each time step and then plotting

them to observe convergence. In the case of oscillatory convergence the average of a suitably large number of the oscillatory steady values can be taken. This is what is done in the current study. Discretization error, u_h , is a consequence of the transformation of the continuum equations into a system of algebraic equations. The ASME Standard recommends the use of Roache's GCI method to estimate this quantity. As described in the ASME Standard [2], the iteration convergence is at least two orders of magnitude smaller than the discretization error estimate:

$$u_{num} = u_h \tag{3.7}$$

otherwise

$$u_{num} = u_h + u_i \tag{3.8}$$

Usually the discretization error is the dominant contribution.

As the GCI method uses Richardson extrapolation, it is necessary for the local values to follow a smooth, monotonic dependence on grid resolution. Determination of the GCI is a five step procedure. The first is to define the cell size. In order to define the cell, mesh or grid size, this problem will consider the non-structured grid (since it is assumed that the grids will not be exactly geometrically similar). The formula for estimating the grid size, *h, is:*

$$h = \left[\frac{(\sum_{i=1}^{N} \Delta V_i)}{N}\right]^{\frac{1}{3}} \tag{3.9}$$

where *N* is the total number of cells and ΔV_i is the volume of the i^{th} cell.

At least three different grid sizes are required since the order of convergence, *p*, is unknown. The second step, therefore is to determine the Grid Refinement Factors (GRF), r_{32} and r_{21}. If we let

$$h_1 < h_2 < h_3 \tag{3.10}$$

$$r = \frac{h_{coarse}}{h_{fine}}, \tag{3.11}$$

$$r_{21} = \frac{h_2}{h_1}, \tag{3.12}$$

$$\text{and } r_{32} = \frac{h_3}{h_2} \tag{3.13}$$

These values should be greater than 1.3 for practical problems (based on Celik et al. [29]) and the refinement should be structured, even if the grid is not. This not being the case could increase convergence time.

The third step is to calculate the apparent order, p, as follows.

$$p = \left[\frac{1}{\ln(r_{21})}\right]\left[\ln\left|\frac{\varepsilon_{32}}{\varepsilon_{21}}\right| + q(p)\right] \tag{3.14}$$

where

$$q(p) = \ln\left(\frac{r_{21}^p - s}{r_{32}^p - s}\right), \tag{3.15}$$

$$s = 1 \cdot sign\left(\frac{\varepsilon_{32}}{\varepsilon_{21}}\right), \tag{3.16}$$

$$\varepsilon_{32} = \varphi_3 - \varphi_2 \text{ and} \tag{3.17}$$

$$\varepsilon_{21} = \varphi_2 - \varphi_1 \tag{3.18}$$

The values $\varphi_1, \varphi_2$and $\varphi_3$are the numerical solution results of the quantity for which the final uncertainty is desired. The solution requires an initial guess for $q(p)$ which is usually taken to be zero.

Step four involves determining the extrapolated values φ_{ext}^{21}, using

$$\varphi_{ext}^{21} = \frac{(r_{21}^{p}\varphi_1 - \varphi_2)}{(r_{21}^{p} - 1)} \tag{3.19}$$

Step five requires calculating and reporting the error estimates $e_a^{21}$and e_{ext}^{21}using the observed p value (using dimensional form).

$$e_a^{21} = |\varphi_1 - \varphi_2| \text{ and} \tag{3.20}$$

$$e_{ext}^{21} = \left|\frac{\varphi_{ext}^{21} - \varphi_1}{\varphi_{ext}^{21}}\right| \tag{3.21}$$

The next step in the calculation is to determine the Grid Convergence Index, GCI_{fine}^{21} as

$$GCI_{fine}^{21} = \frac{F_s \cdot e_a^{21}}{r_{21}^{p} - 1}. \tag{3.22}$$

This equation gives the GCI applicable to the fine grid or that corresponding to h_1 which is usually the grid used to report the answer to the problem. Since this GCI corresponds to the solution obtained with h_1 and was determined using the results of grids corresponding to h_1 and h_2, it is given the symbol, GCI_1^{21}. Roache [12] also presents an equation for the GCI applicable to the coarse grid corresponding to h_2 which is based on solutions obtained using the results of grids corresponding to h_1 and h_2, as:

$$GCI_2^{21} = GCI_{coarse}^{21} = \frac{F_s \cdot e_a^{21} r_{21}^p}{r_{21}^p - 1} \tag{3.23}$$

Another estimate can be made of this GCI value for the solution obtained with h_2 that was determined using the results of grids corresponding to h_2 and h_3 as

$$GCI_2^{32} = GCI_{fine}^{32} = \frac{F_s \cdot e_a^{32}}{r_{32}^p - 1} \tag{3.24}$$

In this case φ_{ext}^{21}, e_a^{21} and e_{ext}^{21} are calculated using equations (3.19) to (3.21) inclusive except that the 2's are replaced by 3's and the 1's are replaced by 2's. In order to solve for p, GCI_{fine}^{32} and GCI_{coarse}^{21} are equated. This assumes that the p is equal for both GCI values.

Likewise an estimate can be made of the GCI value for the solution obtained with h_3 that was determined using the results of grids corresponding to h_2 and h_3 as

$$GCI_3^{32} = GCI_{coarse}^{32} = \frac{F_s \cdot e_a^{32} r_{32}^p}{r_{32}^p - 1} \tag{3.25}$$

Since the solution of interest in this study is that determined using h_3, GCI_3^{32} is used to determine u_h as follows

$$u_h = S_j * \frac{GCI_3^{32}}{2} \tag{3.26}$$

where the factor "2" is referred to as an expansion factor associated with the confidence level of the uncertainty [2]. The last step is to calculate u_{num} using equation (3.8).

In this thesis, calculations are done for four different grid sizes. The reasons for the four grids will be discussed in the results section. As mentioned previously, the four values of *N* are 5576928, 1834309, 716538 and 229766. It is not practical to consider the

uncertainty at all of the solution points and hence six points on one pole were selected for study. These are the points at heights of 0.1, 0.6, 1.1, 1.5, 1.9 and 2.3 m on pole 4. The average values of the last 400 time steps, as described previously, were used as the final steady state values.

3.3.4 Procedure for Obtaining the Uncertainty in the Experimental Results, u_D

Finally, the last term required for determining the total uncertainty is that for the experimental results, u_D. As noted in the beginning of this chapter, hot-sphere anemometers with a probe size of 3.175 mm (1/8 inch) were used in the experiment, with a measurement range of 0.05 to 5 m/s and a repeatability of 2%. Thus, the uncertainty due to this equipment is calculated as follows:

$$u_D = 0.02 * S_j \tag{3.27}$$

where S_j is defined in Section 3.3.2 as the average velocity over the last 400 values. At each height along the pole, the uncertainty due to the experimental equipment is calculated from this equation.

CHAPTER 4 Results and Discussion

In this chapter the results of the numerical experiments outlined in Section 3.3 are presented and discussed. The information is organized into sub-sections in the same manner as in that chapter.

4.1 Determining Steady State Values and Selection of Specific Points of Consideration

The predicted velocity results are obtained for all of the 54 measuring points mentioned previously using mesh N3. It is not practical to attempt a presentation of all of the results; hence the results of predicted velocity at one specific pole location, number 4, are given in Figure 4.1 which covers a time span of 5400 seconds or 90 minutes.

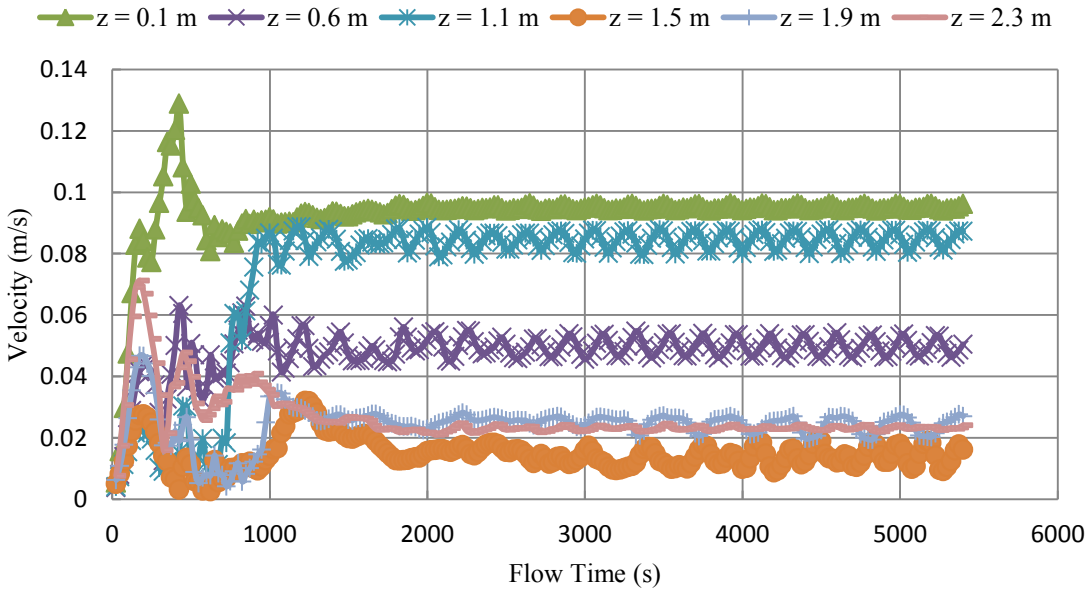

Figure 4.1 Pole location number 4: velocity vs. time plot [30]

The existence of oscillatory convergence is observed and the final value depends where the oscillatory convergence plot ends. Comparisons of only the final values would lead to erroneous conclusions. In order to quantify the degree of convergence, results in sets of 400 consecutive seconds were grouped and averaged. This time interval was

determined by increasing the number of seconds until the changes in the average were negligible. The comparison of consecutive group averages revealed that the change in velocity values for all heights at all pole locations was below 0.25%. The pole location which had the lowest change was pole location number 4, which gave a change of only 0.03% of the previous value. In order to minimize the effect of these differences on further calculations only pole location number 4 will be considered further in this study.

The nominal values of the simulated velocities and experimental data can be found in Figure 4.2. In the next sections, the uncertainties will be reviewed and analyzed, to determine if they can explain the discrepancies between simulated and experimental results.

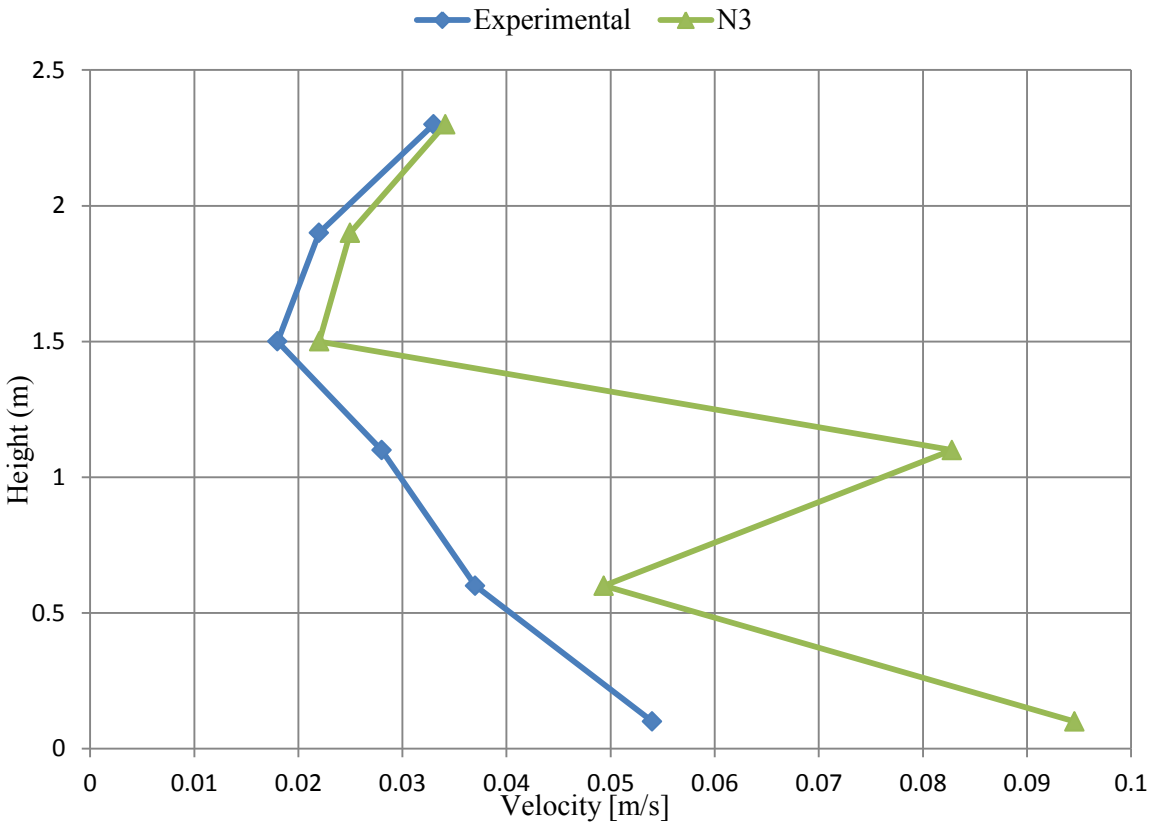

Figure 4.2 Experimental velocity vs. simulated velocity on pole 4

4.2 Input Parameter Sensitivity Study and Input Uncertainty, u_{input}

The S_{ji}^{-} and S_{ji}^{+} values for each of the 6 input parameters as well as the baseline, S_{ji}, value are determined using the Fluent solution previously mentioned with the N3 grid. The different terms in equation (3.6), as discussed in Section 3.3.2, are then used to determine the total uncertainty caused by uncertainties in each of the input quantities.

Table 4.1 presents the square of these values for all of the parameters used at each specific point on pole 4. The percent contribution for each parameter is shown in brackets. These values are tallied at the bottom of the chart for the combined overall effect. Analyzing the data indicates that the largest contribution to the input uncertainty depends on the measured location on the pole.

Analyzing the averages of the percentage values over all locations on the pole indicates that the temperatures of the walls, floor and ceiling have the highest average effect with a value of 41.6% followed by the heat source values at 37.4% and finally by the inlet velocity with 19.2%. The effect of the heat sources is dominant near the lower portion of the pole (due to the pole's close proximity to the heat sources at these locations), while the higher end of the pole proves to have dominant effect from the temperatures of the walls, floor and ceiling. The only exception is at height 1.9 m, where the inlet velocity is the most prominent. As for the inlet temperature and turbulence values, they appear to have an overall negligible effect on this pole.

The nominal values of the simulated velocities and experimental data can be found in Figure 4.3. The input uncertainty values, u_{input} , at each height on the pole 4 are represented by the error bars. It is noted that at heights of 0.1 m and 1.1 m, the simulated data with the error bar falls out of the uncertainty range versus the experimental. This

indicates that the input uncertainty error bar alone is not capable of accounting for the difference in the simulated result when compared with the experimental data at these points. In the next sections, the numerical and experimental uncertainties will be reviewed and analyzed, with the intent to determine if the discrepancies between simulated and experimental can be attributed to either of these uncertainties.

Table 4.1 Contribution of input uncertainties in velocity at pole 4 [30]

Simulation Input, X_i		Contribution to Input Uncertainty in Inlet, $(u_{input})^2$, *(% of total)* at each Height Location (m/s)^2					
		0.1	0.6	1.1	1.5	1.9	2.3
Inlet	Velocity	2.337E-05 (24.7)	7.491E-08 (0.0)	7.707E-05 (21.6)	1.622E-07 (0.7)	9.103E-07 (58.8)	1.780E-06 (9.5)
	Temperature	3.212E-06 (3.4)	9.390E-06 (1.8)	5.635E-07 (0.1)	1.135E-06 (4.8)	8.027E-10 (0.1)	1.283E-08 (0.1)
	Turbulence Intensity	1.416E-08 (0.0)	3.868E-09 (0.0)	1.427E-09 (0.0)	1.844E-11 (0.0)	1.690E-12 (0.0)	1.131E-11 (0.0)
	Hydraulic Diameter	4.689E-13 (0.0)	3.167E-12 (0.0)	2.338E-12 (0.0)	1.908E-11 (0.0)	3.641E-13 (0.0)	4.810E-15 (0.0)
Walls, Floor & Ceiling		2.002E-05 (21.2)	1.318E-05 (2.5)	1.873E-07 (0.1)	2.252E-05 (94.5)	6.379E-07 (41.1)	1.703E-05 (90.4)
Heat Sources		4.787E-05 (50.7)	5.111E-04 (95.7)	2.798E-04 (78.2)	4.929E-12 (0.0)	1.184E-12 (0.0)	1.927E-14 (0.0)
Overall or Total		9.449E-05	5.337E-04	3.576E-04	2.382E-05	1.549E-06	1.883E-05

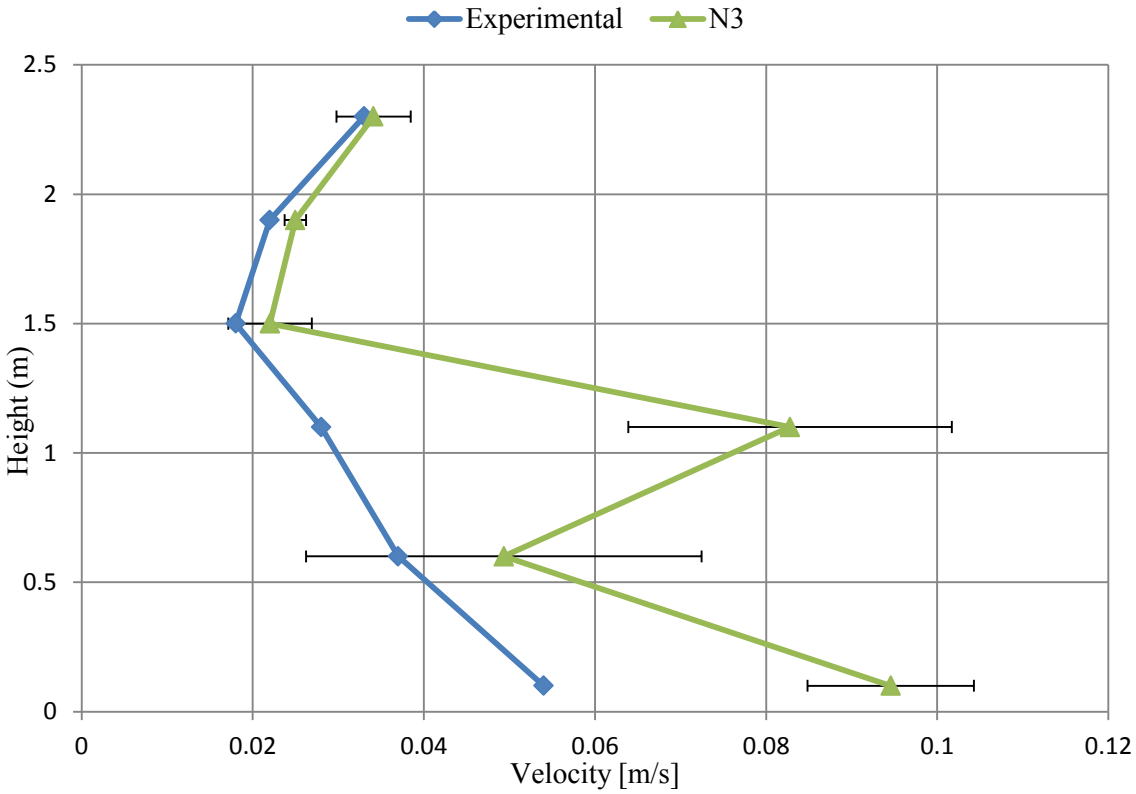

Figure 4.3 Experimental velocity vs. simulated velocity with error bars on pole 4 [30]

4.3 GCI Study and Numerical Uncertainty, u_{num}

This section presents the results for the calculation of the numerical uncertainty in the simulation as discussed in section 3.3.3. The values of *h*determined using equation (3.8) and corresponding to each of the meshes can be found in Table 4.2.

Table 4.2 GCI *h* values at different mesh sizes

Mesh	*h* (m)
N1	1.986E-02
N2	2.877E-02
N3	3.936E-02
N4	5.750E-02

The next step in the procedure involves a determination of the GRF values for this study which are calculated using equations (3.12) and (3.13) and tabulated in Table 4.3.

These meet the ASME Standard guidelines since the GRF for each case is above the required value of 1.3.

Table 4.3 Grid refinement factor values

GRF	
r_{21}	1.461
r_{32}	1.368
r_{43}	1.449

Step 3 is a determination of the observed order, p. This requires calculation of the values of ε_{21}, ε_{32}, s and $q(p)$ using equations (3.14) thru (3.18) in Chapter 3. The values required in the calculation and the resulting values are presented in Table 4.4.

The GCI_{coarse}^{32} values are also determined using equation (3.25) and included in Table 4.4. These are required to estimate the uncertainty associated with grid N3 and are also used in determining the u_{input}. The values φ_{ext}^{32} and e_{ext}^{32} are quantities included in the ASME Standard but not used in the determination of the uncertainty. They are included in Table 4.4 for completeness.

Table 4.4 GCI uncertainty analysis values – grids N1, N2 & N3

Variable	Height (m)					
	0.1	0.6	1.1	1.5	1.9	2.3
φ_1 (m/s)	8.858E-02	4.537E-02	2.267E-02	1.185E-02	1.623E-02	3.922E-02
φ_2 (m/s)	9.307E-02	4.707E-02	5.699E-02	1.961E-02	2.413E-02	3.384E-02
φ_3 (m/s)	9.458E-02	4.930E-02	8.284E-02	2.194E-02	2.494E-02	3.418E-02
ε_{21} (m/s)	4.495E-03	1.698E-03	3.432E-02	7.768E-03	7.895E-03	-5.374E-03
ε_{32} (m/s)	1.509E-03	2.238E-03	2.585E-02	2.330E-03	8.169E-04	3.394E-04
s	1	1	1	1	1	-1
p	-2.664	1.295	-0.342	-2.984	-5.969	-7.335
$q(p)_{32}$	1.015E-01	2.052E-01	1.562E-01	9.527E-02	5.050E-02	3.688E-02
φ_{ext}^{32}	9.573E-02	4.262E-02	3.101E-01	2.344E-02	2.509E-02	3.422E-02
e_a^{32}	1.622%	4.755%	45.362%	11.880%	3.386%	1.003%
e_{ext}^{32}	2.777%	10.428%	81.624%	16.320%	3.843%	1.101%
GCI_{coarse}^{32}	**-1.544%**	**17.748%**	**-498.518%**	**-9.528%**	**-0.763%**	**-0.138%**

From the values in this table the following points are noted.

1) For a height of 2.3 m, the s value is -1 indicating a non-monotonic condition.
2) At certain heights the value of p and hence GCI are negative. A search of the literature indicates that negative p values, although undesirable, are possible. In fact, a paper [29], by many of the same authors of the ASME Standard, published just one year before the Standard was published, used a slightly different equation for p as indicated below

$$p = \left[\frac{1}{ln(r_{21})}\right]\left|ln\left|\frac{\varepsilon_{32}}{\varepsilon_{21}}\right| + q(p)\right| \tag{4.1}$$

The only difference in equation (4.1) and (3.14) is the absolute value of the terms in the second set of parentheses, which are found in equation (4.1).

When recalculating the observed value p and values that depend upon p, the values change considerably. This is evident in Table 4.5, which has very different GCI

values at every height with the exception of 0.6 m. Also, it is evident in the p values, which are mostly negative in Table 4.4, but are all positive in Table 4.5.

Table 4.5 GCI uncertainty analysis values using absolute equation (4.1) – grids N1, N2 & N3 [30]

Variable	Height (m)					
	0.1	0.6	1.1	1.5	1.9	2.3
φ_1 (m/s)	8.858E-02	4.537E-02	2.267E-02	1.185E-02	1.623E-02	3.922E-02
φ_2 (m/s)	9.307E-02	4.707E-02	5.699E-02	1.961E-02	2.413E-02	3.384E-02
φ_3 (m/s)	9.458E-02	4.930E-02	8.284E-02	2.194E-02	2.494E-02	3.418E-02
ε_{21} (m/s)	4.495E-03	1.698E-03	3.432E-02	7.768E-03	7.895E-03	-5.374E-03
ε_{32} (m/s)	1.509E-03	2.238E-03	2.585E-02	2.330E-03	8.169E-04	3.394E-04
s	1	1	1	1	1	-1
p	2.293	1.295	0.294	2.570	5.155	6.532
$q(p)_{32}$	2.393E-01	2.052E-01	1.742E-01	2.493E-01	3.531E-01	3.350E-01
φ_{ext}^{32}	9.165E-02	4.262E-02	-2.098E-01	1.774E-02	2.393E-02	3.379E-02
e_a^{32}	1.622%	4.755%	45.362%	11.880%	3.386%	1.003%
e_{ext}^{32}	1.556%	10.428%	127.160%	10.543%	0.839%	0.147%
GCI_{coarse}^{32}	**3.942%**	**17.748%**	**641.932%**	**26.772%**	**5.273%**	**1.437%**

Because of the non-monotonic nature at a height of 2.3 m, it was decided to utilize another grid triplet to determine the uncertainty value. This requires the generation of one additional grid, N4, for which the h value can be found in Table 4.2. The calculations using the grid triplet N2, N3, & N4 are shown in Table 4.6. In this case, the observed order equation for p utilizes equation (4.1) which includes the absolute value. The equations are the same as used previously except that the 1's are replaced by 2's, the 2's are replaced by 3's and the 3's are replaced by 4's.

In order to estimate the uncertainty of grid N3 using this grid triplet, it is necessary to use grids N4 and N3 to determine the GCI value on grid N3 as indicated below.

$$GCI_3^{43} = GCI_{fine}^{43} = \frac{F_s \cdot e_a^{43}}{r_{43}^p - 1} \tag{4.2}$$

Table 4.6 GCI uncertainty analysis values using absolute equation – grids N2, N3 & N4

Variable	Height (m)					
	0.1	0.6	1.1	1.5	1.9	2.3
φ_2 (m/s)	9.307E-02	4.707E-02	5.699E-02	1.961E-02	2.413E-02	3.384E-02
φ_3 (m/s)	9.458E-02	4.930E-02	8.284E-02	2.194E-02	2.494E-02	3.418E-02
φ_4 (m/s)	8.253E-02	3.836E-02	3.965E-02	2.837E-02	2.965E-02	3.467E-02
ε_{32} (m/s)	1.509E-03	2.238E-03	2.585E-02	2.330E-03	8.169E-04	3.394E-04
ε_{43} (m/s)	-1.205E-02	-1.094E-02	-4.319E-02	6.424E-03	4.708E-03	4.927E-04
s	-1	-1	-1	1	1	1
p	5.608	4.326	1.448	2.365	4.758	0.543
$q(p)_{43}$	-3.120E-01	-2.250E-01	-5.739E-02	-2.695E-01	-2.538E-01	-2.019E-01
φ_{ext}^{43}	9.276E-02	5.195E-02	1.420E-01	1.751E-02	2.401E-02	3.202E-02
e_a^{43}	12.741%	22.191%	52.137%	29.274%	18.874%	1.441%
e_{ext}^{43}	0.336%	5.086%	41.671%	25.350%	3.881%	6.749%
GCI_{fine}^{43}	**2.167%**	**6.699%**	**89.301%**	**25.279%**	**4.670%**	**7.903%**

As observed in Table 4.6, the last three heights are monotonic. In view of this fact, one would expect the calculated GCI to be relatively close to the corresponding monotonic values in the first grid triplet. As expected, the GCI values at 1.5 m, for the first grid triplet is 26.772% which is very close to the 25.279% for the second grid triplet. Also, for a height of 1.9 m, the first grid triplet is 5.273%, whereas the second grid triplet is 4.670%. Finally, the values for the height of 2.3 m are now monotonic in the second grid triplet.

Finally, the u_{num} is calculated by adding the discretization error, u_h and iteration convergence, u_i as indicated in equation (3.8).

All GCI values were calculated using GCI_{coarse}^{32}, except the last height, 2.3 m which uses GCI_{fine}^{43}. These resulting values are shown in Table 4.7.

Table 4.7 Calculation of numerical uncertainty

Variable	Height (m)					
	0.1	0.6	1.1	1.5	1.9	2.3
GCI_{coarse}^{32}	3.942%	17.748%	641.932%	26.772%	5.273%	7.903%
u_i(m/s)	2.906E-05	-1.673E-06	8.468E-06	1.508E-03	7.092E-05	-9.213E-05
u_h (m/s)	1.864E-03	4.375E-03	2.659E-01	2.937E-03	6.576E-04	1.370E-03
u_{num} (m/s)	1.893E-03	4.377E-03	2.659E-01	4.446E-03	7.285E-04	1.462E-03

4.4 Estimation of Experimental Uncertainty, u_D

The experimental uncertainty, u_D, is calculated using equation (3.24), with the same values of S_j used in the parametric study. The results for pole 4 can be found in Table 4.8.

Table 4.8 Uncertainty due to experimental setup at pole 4

Variable	Height (m)					
	0.1	0.6	1.1	1.5	1.9	2.3
φ_3 (m/s)	9.458E-02	4.930E-02	8.284E-02	2.194E-02	2.494E-02	3.418E-02
u_D (m/s)	1.8917E-03	9.8608E-04	1.6567E-03	4.3887E-04	4.9888E-04	6.8364E-04

The largest uncertainty due to experimental setup is at height 0.1 m, which is the highest recorded velocity.

4.5 Total or Overall Uncertainty, u_{total}

Finally, the total or overall uncertainty can be calculated using equation (2.4). All of the values are presented in Table 4.9, which provides the overall uncertainty at the different height locations on pole 4.

Table 4.9 Overall uncertainty along pole 4 heights

Uncertainty (m/s)	Height (m)					
	0.1	0.6	1.1	1.5	1.9	2.3
u_{input}	9.4486E-05	5.3372E-04	3.5762E-04	2.3817E-05	1.5490E-06	1.8825E-05
u_{num}	-7.010E-04	4.374E-03	-2.065E-01	4.630E-04	-2.422E-05	-1.158E-04
u_D	1.892E-03	9.861E-04	1.657E-03	4.389E-04	4.989E-04	6.836E-04
u_{total}	9.9275E-03	2.3533E-02	2.0735E-01	4.9217E-03	1.3411E-03	4.3938E-03

Based on the total uncertainty that was calculated, the error bars are now indicated with the previous results for velocity and presented in Figure 4.4. The results indicate that the discrepancy between the experimental and CFD simulated results can be attributed to the overall uncertainty at all points on the pole except for the one closest to the floor. A possible reason for this discrepancy could be the way the numerical model treats conditions at the wall.

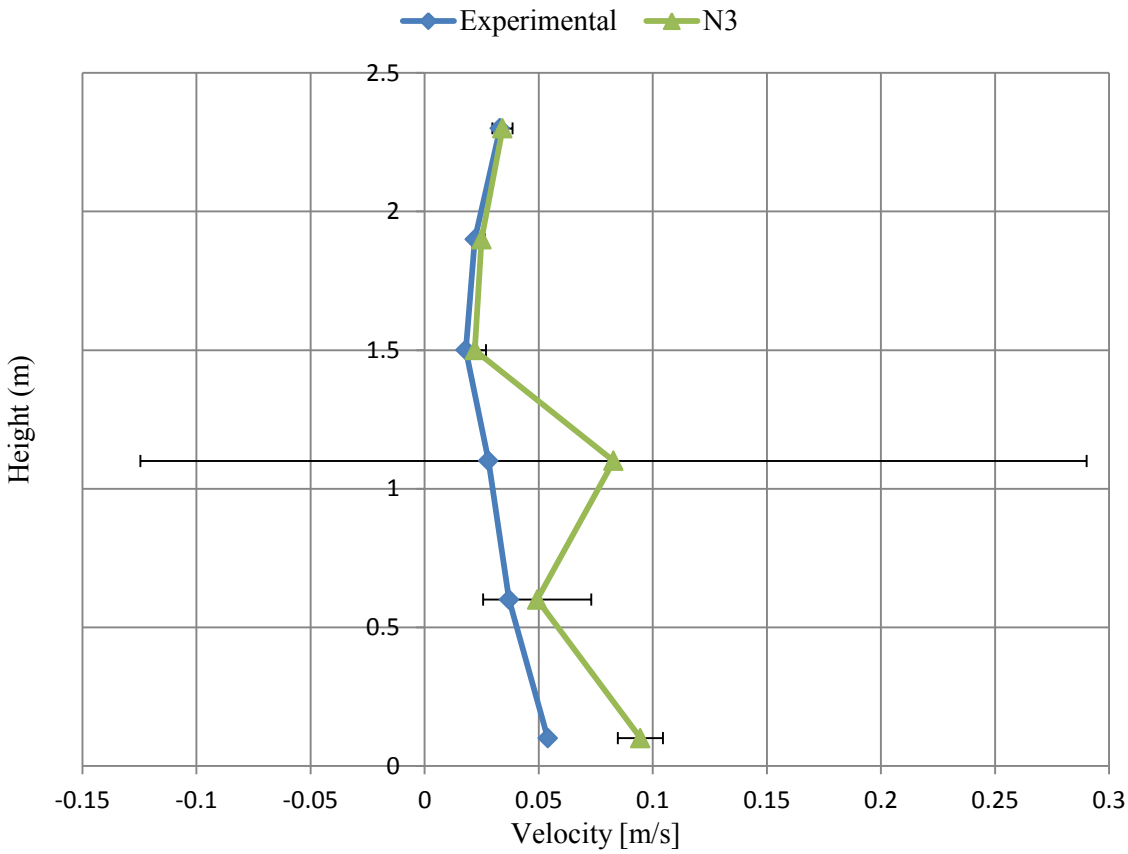

Figure 4.4 Experimental vs. CFD simulated (mesh N3) with error bars

4.6 Analysis of the Flow Field Around an Anomalous Point

Although the uncertainties in the numerical solution are capable of explaining almost all of the differences between the experimental and numerical results, it is of interest to investigate the changes in the flow field that account for the large changes in the velocity at a height of 1.1 m. As seen previously in Figure 4.4, the simulated result at this location provides the largest discrepancy when comparing to the experimental results. However, as the mesh gets finer (from N3 to N1), the difference reduces. The intent of this section is to investigate changes in the flow field that occur with changes in the grid size to understand the phenomena occurring at this location.

To accomplish this, stream traces of particles which pass through the point of interest are shown within a one meter cubed volume surrounding the focused point for each of the N3 (grid used in the study) , N2 (a finer grid) and N1 (the finest grid) grids. In order to better understand the changes in the flow patterns the stream traces were observed in the x-y, z-y and z-x planes as well as with a perspective view. All of the stream trace views can be found in Appendix D. The isometric views of the stream traces for meshes N1, N2 and N3 for the height of 1.1 m which exhibited an anomalous behaviour and 1.5 m which is the height immediately next to 1.1 m are presented in Figure 4.5 and 4.6, respectively. In the case of the 1.1 m height, the change in shape and direction of the stream trace as the mesh size is decreased are clearly seen by comparing Figures 4.5 a, b and c. The flow changes from passing around the nearby occupant to up and over it as the grid size is reduced. For the next height location up, 1.5 m, no such change in direction is noticed. It is therefore concluded that the influence of grid size on the flow pattern over the occupant closest to the point in question at the height of 1.1 m, is related to the discrepancy witnessed between the different meshes.

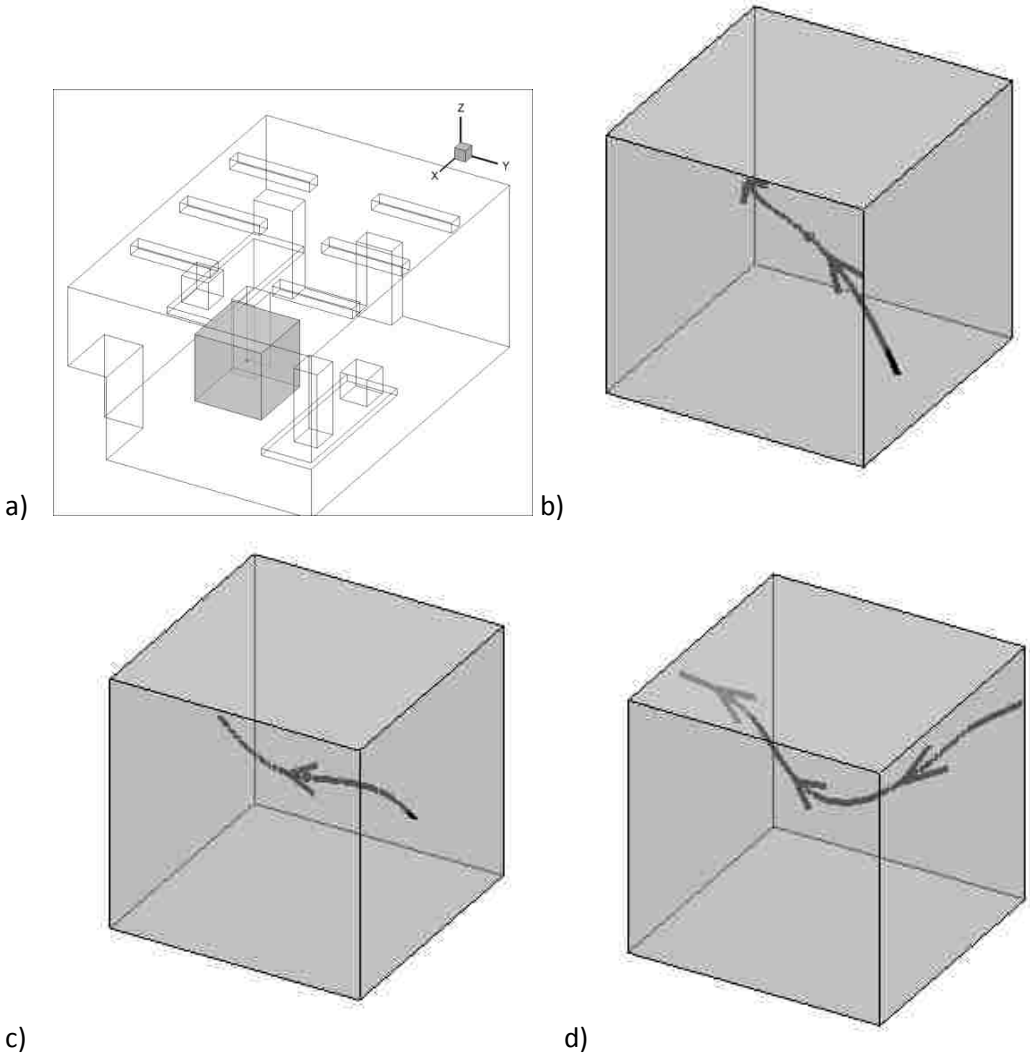

Figure 4.5 Isometric view of anomalous point on pole 4 – height of 1.1 m; a) location of stream trace, b) mesh N3, c) mesh N2, d) mesh N1

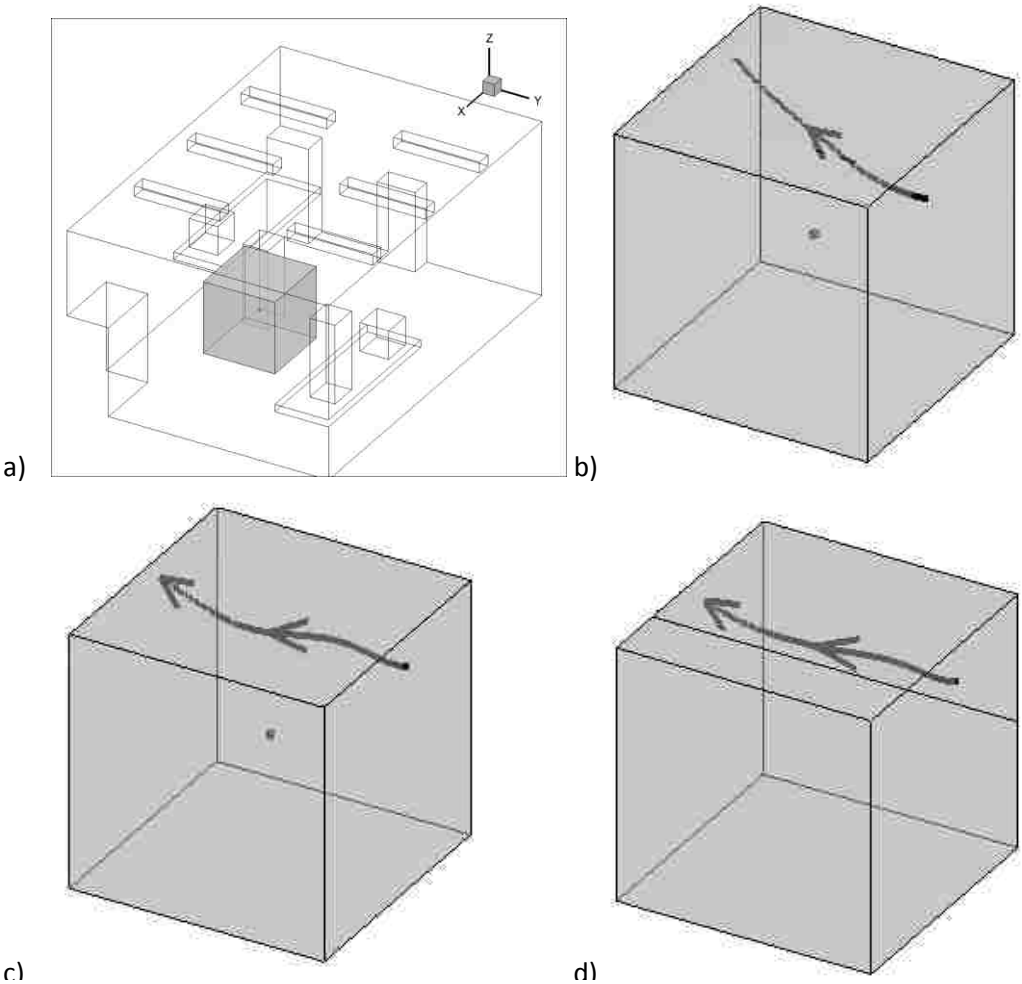

Figure 4.6 Isometric view of anomalous point on pole 4 – height of 1.5 m; a) location of stream trace, b) mesh N3, c) mesh N2, d) mesh N1

The technique for determining the numerical uncertainty described in the ASME V&V 20-2009 Standard was investigated in detail and applied with some modifications, to the case of a computational fluid dynamic solution of the flow pattern within a small office space. The technique comprised of determining the three parts of the uncertainty: the experimental measurements, the input parameters and the numerical model. Details of the changes in the flow pattern around a point which exhibited an anomalous behaviour with changes in grid size were also investigated.

CHAPTER 5 Conclusions and Recommendations

Conclusions regarding each of these factors as well as general conclusions are presented below.

The uncertainty in the experimental measurements alone was not capable of explaining the differences between the computational and numerical results.

The input uncertainty alone was also not capable of explaining the differences between the numerical and experimental results.

Regarding the influence of specific types of input uncertainty, it was found that:

1. Considering pole average values, the temperatures of the walls, floor and ceiling have the highest average effect with a value of 41.6% followed by the heat source values at 37.4% and finally by the inlet velocity with 19.2%.
2. Generally, the effect of the heat sources on velocity are dominant near the lower portion of the pole (due to the pole's close-proximity to the heat sources at these locations), while the temperatures of the walls, floor and ceiling have a dominant effect on the upper end of the pole. The only exception is at height of 1.9 m, where the inlet velocity is the most prominent.
3. The inlet temperature and turbulence values have a negligible effect.

In the process of determining the model uncertainty it was discovered that:

1. Although not explicitly stated in the Standard, the model uncertainty (and hence GCI value) must be estimated for the same grid size used for estimating the input and other uncertainties.

2. GCI values required for determining the model uncertainty require that the results for the three different grid sizes vary in a monotonic manner which may preclude model uncertainty estimation with those grids.
3. If adjacent grid triplets are each monotonic, the GCI values determined at shared points have approximately the same value regardless of which grid triplet is used.
4. Where it is not possible to estimate the GCI value using the GCI_{fine} formula with a particular set of grids it is possible to estimate the GCI value for that grid size by performing one more calculation at a different grid size and use the formula for GCI_{coarse}.

In general it can be concluded that

1. Combination of the experimental, input and model uncertainties is capable of explaining the differences between the numerical and experimental data at all but the lowest height on pole 4.
2. The unexplained differences between the experimental and numerical results near the floor are speculated to be due to invalid assumptions being made in modelling the flow near the floor. This is evident when observing the experimental data versus N1, N2 and N3, which can be found in Appendix E. As the grid gets finer, the velocity at the closest point on the floor hardly changes.
3. A careful study of the flow pattern changes with mesh size around the anomalous point at height 1.1 m was found to be due to the solution inaccuracies in close proximity of a geometrical shape in the room (one of the occupants).

Finally, use of the ASME V&V 20-2009 Standard has been shown to be a useful aid in explaining the differences between experimental and numerical measurements in indoor spaces.

5.1 Recommendations for Use of the ASME Standard

From the experiences gained during the course of this work, the following recommendations are made regarding the use of the ASME V&V 20-2009 Standard:

1. Although not specifically mentioned in the Standard, it is obvious that the contribution to the uncertainty due to the input parameters and boundary conditions, u_{input} , must be evaluated using the same grid used to determine the contribution due to the numerical aspects such as iteration convergence and grid spacing, u_{num}.
2. The equations provided in the Standard for determining u_{num} using the GCI approach only mention GCI_{fine}^{21}, which applies to the smaller of the two grids used in its determination. In order to satisfy the condition in point #1 above, this means that the sensitivity study used to determine u_{input} must be done on the fine grid, which is very time consuming. This might not be feasible in industry depending upon the particular case.
3. Using the value of GCI_{coarse}^{32} , as done in this thesis, avoids this problem while still providing an estimate of the uncertainty in the result.
4. The importance of obtaining monotonicity of the solution results, as indicated in the early papers dealing with the GCI, is not explicitly stated in the Standard and should be noted by its users.

5. Determination of the approximate order of the equations, p, associated with obtaining the GCI value, should be evaluated using the absolute value as indicated in equation (4.1). This procedure provides estimates of the uncertainty of the numerical calculation for a particular grid size, using larger and smaller grids, which are close to one another.

REFERENCES

[1] ASHRAE Handbook Committee, 2009, "2009 ASHRAE Handbook Fundamentals," ASHRAE.

[2] V & V 20 Committee, 2009, "Standard for Verification and Validation in Computational Fluid Dynamics and Heat Transfer," ASME, USA.

[3] Freitas, C. J., 1999, "The Issue of Numerical Uncertainty," Second International Conference on CFD in the Minerals and Process Industries, CSIRO, December 6-8, Melbourne, Australia, pp. 29-34.

[4] Kline, S. J., Morkovin, M. V., Sovran, G., 1968, "Computation of Turbulent Boundary Layers – 1968 AFOSR-IFP-Stanford Conference, Volume 1," Conference on Computation of Turbulent Boundary Layers, August 19-24, Stanford, CA, USA.

[5] Ghia, K. N., Mueller, T. J., Patel, B. R., 1981, "Computers in Flow Predictions and Fluid Dynamics Experiments, "Winter Annual Meeting of ASME," November 15-20, Washington, D.C., USA.

[6] Richardson, L. F., 1910, "Approximate Arithmetical Solution of Physical Problems Involving Differential Equations," Philosophical Transactions of the Royal Society of London, 210 pp. 307-357.

[7] Pletcher, R.H., Tannehill, J.C., Anderson, D., 2012, "Computational Fluid Mechanics and Heat Transfer," Taylor & Francis, USA .

[8] Slater, J. W., 2008, "Examining Spatial (Grid) Convergence " http://www.grc.nasa.gov/WWW/wind/valid/tutorial/spatconv.html Accessed 2014 (02/21), NPARC Alliance CFD Verification and Validation.

[9] AIAA Committee, 1998, "AIAA Guide for the Verification and Validation of Computational Fluid Dynamics Simulations (G-077-1998e)," AIAA

[10] Oberkampf, W. L., Blottner, F. G., 1998, "Issues in Computational Fluid Dynamics Code Verification and Validation," AIAA Journal, 36(5) pp. 687-695.

[11] Karniadakis, G. E., 1995, "Toward a Numerical Error Bar in CFD," ASME Journal of Fluids Engineering, 117(1) pp. 7-9.

[12] Roache, P.J., 1998, "Verification and Validation in Computational Science and Engineering," Hermosa Publishers, Albuquerque, New Mexico, USA.

[13] Chen, Q., Lee, K., Mazumdar, S., 2010, "Ventilation Performance Prediction for Buildings: Model Assessment," Building and Environment, 45(2) pp. 295-303.

[14] Chen, Q., 2009, "Ventilation Performance Prediction for Buildings: A Method Overview and Recent Applications," Building and Environment, 44(4) pp. 848-858.

[15] Nielsen, P. V., Restivo, A., Whitelaw, J. H., 1978, "The Velocity Characteristics of Ventilated Rooms," ASME Journal of Fluids Engineering, 100(3) pp. 291-298.

[16] Nielsen, P. V., 1975, "Prediction of Air Flow and Comfort in Air Conditioned Spaces," ASHRAE Transactions, 81(2) pp. 247-259.

[17] Blanes-Vidal, V., Guijarro, E., Balasch, S., 2008, "Application of Computational Fluid Dynamics to the Prediction of Air Flow in a Mechanically Ventilated Commercial Poultry Building," Biosystems Engineering, 100(1) pp. 105-116.

[18] Bustamante, E., Garcia-Diego, F., Calvet, S., 2013, "Exploring Ventilation Efficiency in Poultry Buildings: The Validation of Computational Fluid Dynamics (CFD) in a Cross-Mechanically Ventilated Broiler Farm," Energies, 6(5) pp. 2605-2623.

[19] Mistriotis, A., de Jong, T., Wagemans, M., 1997, "The Analysis of Ventilation and Indoor Microclimate in Agricultural Buildings by Computational Fluid Dynamics " Netherlands Journal of Agricultural Science, 45 pp. 81-96.

[20] van Hooff, T., Blocken, B., 2012, "Full-Scale Measurements of Indoor Environmental Conditions and Natural Ventilation in a Large Semi-Enclosed Stadium: Possibilities and Limitations for CFD Validation," Journal of Wind Engineering and Industrial Aerodynamics, 104-106, pp. 330-341.

[21] Chen, Q., Glicksman, L.R., Yuan, X., 1999, "Performance Evaluation and Development of Design Guidelines for Displacement Ventilation," ASHRAE, RP-949, MIT, USA.

[22] ANSYS, 2010, "ANSYS FLUENT 13.0 User's Guide," .

[23] Yuan, X., Chen, Q., Glicksman, L. R., 1999, "Measurements and Computations of Room Airflow with Displacement Ventilation," ASHRAE Transactions, 105(1) pp. 340-352.

[24] CFD Wiki, 2010, "RNG k-Epsilon Model," http://www.cfd-online.com/Wiki/RNG_k-epsilon_model Accessed 2014(02/21) .

[25] Zhang, T., Lee, K., Chen, Q., 2009, "A Simplified Approach to Describe Complex Diffusers in Displacement Ventilation for CFD Simulations," Indoor Air, 19(3) pp. 255-267.

[26] CFD Wiki, 2008, "Hydraulic Diameter," http://www.cfd-online.com/Wiki/Hydraulic_diameter Accessed 2014(02/21) .

[27] Villermaux, E., 1995, "Memory-Induced Low Frequency Oscillations in Closed Convection Boxes," Physical Review Letters, 75(25) pp. 4618-4618.

[28] Wikimedia Foundation, I., 2014, "Mains Electricity," http://en.wikipedia.org/wiki/Mains_electricity Wikipedia, Accessed 2014(02/21) .

[29] Celik, I. B., Ghia, U., Roache, P. J., 2008, "Procedure for Estimation and Reporting of Uncertainty due to Discretization in CFD Applications," ASME Journal of Fluids Engineering, 130(7) pp. 1-4.

[30] Aczel, A., Karimi, M. and Rankin, G.W., 2013, "Effect of Boundary Conditions on Room Ventilation Simulation Uncertainty", International Journal of Surface Engineering & Materials Technology, Vol. 3 No. 1, pp 34-38.

APPENDIX A

Authorization
Buta Singh Sidhu to: Gary Rankin 03/08/2014 07:38 PM
Cc: hazoor sidhu

Dear Professor Rankin,

As Editor-in-chief of the International Journal of Surface Engineering and Materials Technology (IJSEMT) ISSN(Print): 2249-7250, I hereby give yourself and your co-authors permission to use the information, including figures, contained in the journal paper given below in any future published documents with the understanding that complete reference be made to the original publication in IJSEMT.

"Effect of Boundary Conditions on Room Ventilation Simulation Uncertainty"
Aaron A. Aczel, Mo Karimi and Gary Rankin
International Journal of Surface Engineering & Materials Technology, Vol. 3 No. 1 January-June 2013.

Thank you for your support of this journal.

Dr. Buta Singh Sidhu
Dean Academics and International Collaborations
PTU, Jalandhar (Punjab)
India-144601
Ph.: +911822662562
Fax: +911822662573

APPENDIX B

Table B.1 Object sizes

Item	Dimension (m)		
	Length, Δx	Width, Δy	Height, Δz
Room	5.16	3.65	2.43
Window	0.02	3.35	1.16
Diffuser	0.28	0.53	1.11
Exhaust	0.43	0.43	0
Occupants	0.4	0.35	1.1
Computers	0.4	0.4	0.4
Tables	2.23	0.75	0.01
Cabinet 1	0.33	0.58	1.32
Cabinet 2	0.95	0.58	1.24
Lights	0.2	1.2	0.15

APPENDIX C

Table C.1 Location of objects within the room [21]

Item	Dimension (m)			Location (m)		
	Length, Δx	Width, Δy	Height, Δz	Length, Δx	Width, Δy	Height, Δz
Room	5.16	3.65	2.43	0	0	0
Window	0.02	3.35	1.16	5.16	0.15	0.94
Diffuser	0.28	0.53	1.11	0	1.51	0.03
Exhaust	0.43	0.43	0	2.365	1.61	2.43
Occupant 1	0.4	0.35	1.1	1.98	0.85	0
Occupant 2	0.4	0.35	1.1	3.13	2.45	0
Computer 1	0.4	0.4	0.4	1.98	0.1	0.74
Computer 2	0.4	0.4	0.4	3.13	3.15	0.74
Table 1	2.23	0.75	0.01	0.35	0	0.74
Table 2	2.23	0.75	0.01	2.93	2.9	0.74
Cabinet 1	0.33	0.58	1.32	0	0	0
Cabinet 2	0.95	0.58	1.24	4.21	0	0
Light 1	0.2	1.2	0.15	1.03	0.16	2.18
Light 2	0.2	1.2	0.15	2.33	0.16	2.18
Light 3	0.2	1.2	0.15	3.61	0.16	2.18
Light 4	0.2	1.2	0.15	1.03	2.29	2.18
Light 5	0.2	1.2	0.15	2.33	2.29	2.18
Light 6	0.2	1.2	0.15	3.61	2.29	2.18

APPENDIX D

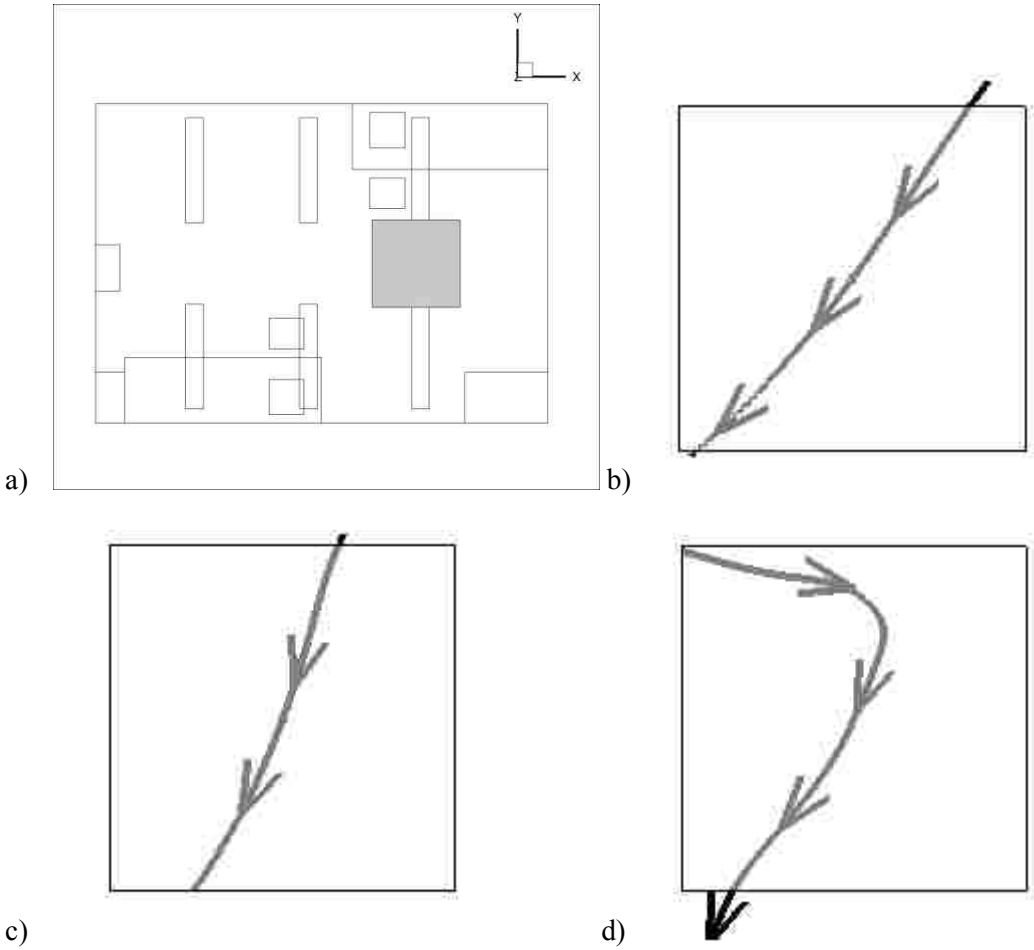

Figure D.1 XY Plane view of an anomalous point on pole 4 – height of 1.1 m; a) location of stream trace, b) mesh N3, c) mesh N2, d) mesh N1

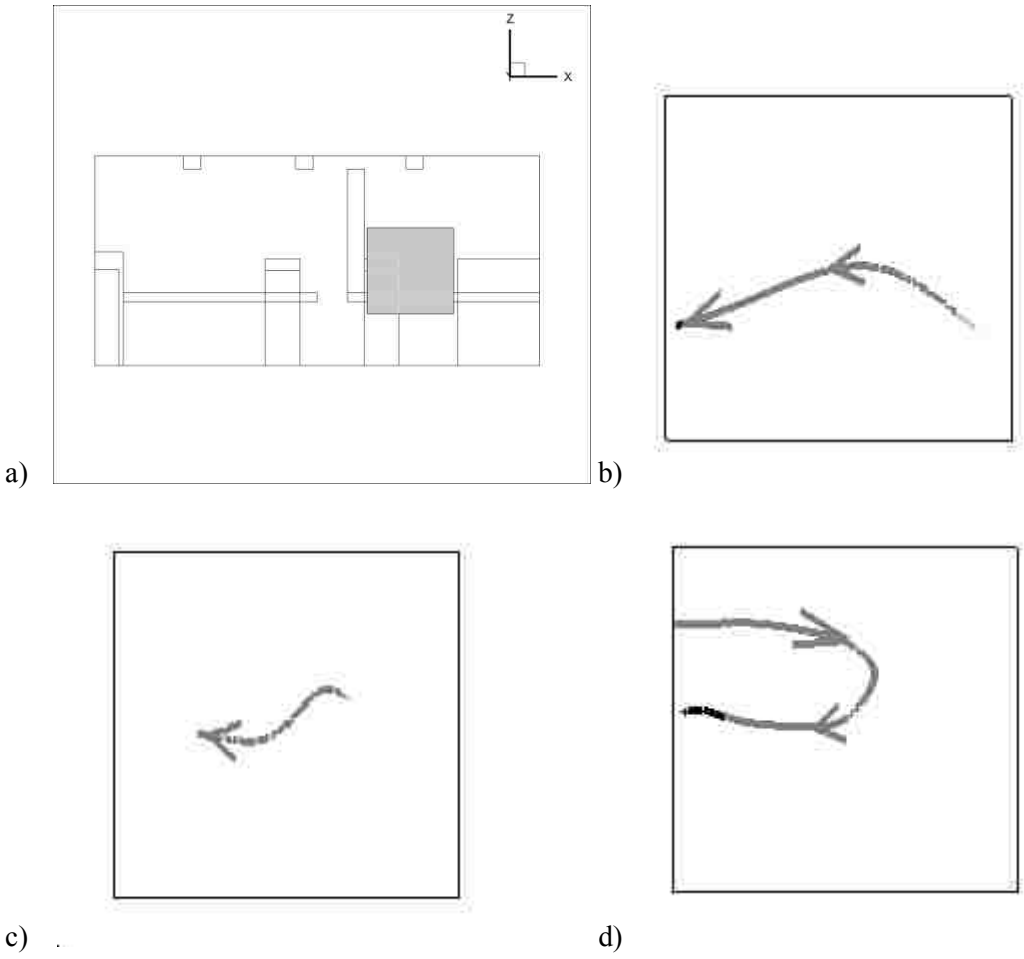

Figure D.2 ZX Plane view of an anomalous point on pole 4 – height of 1.1 m; a) location of stream trace, b) mesh N3, c) mesh N2, d) mesh N1

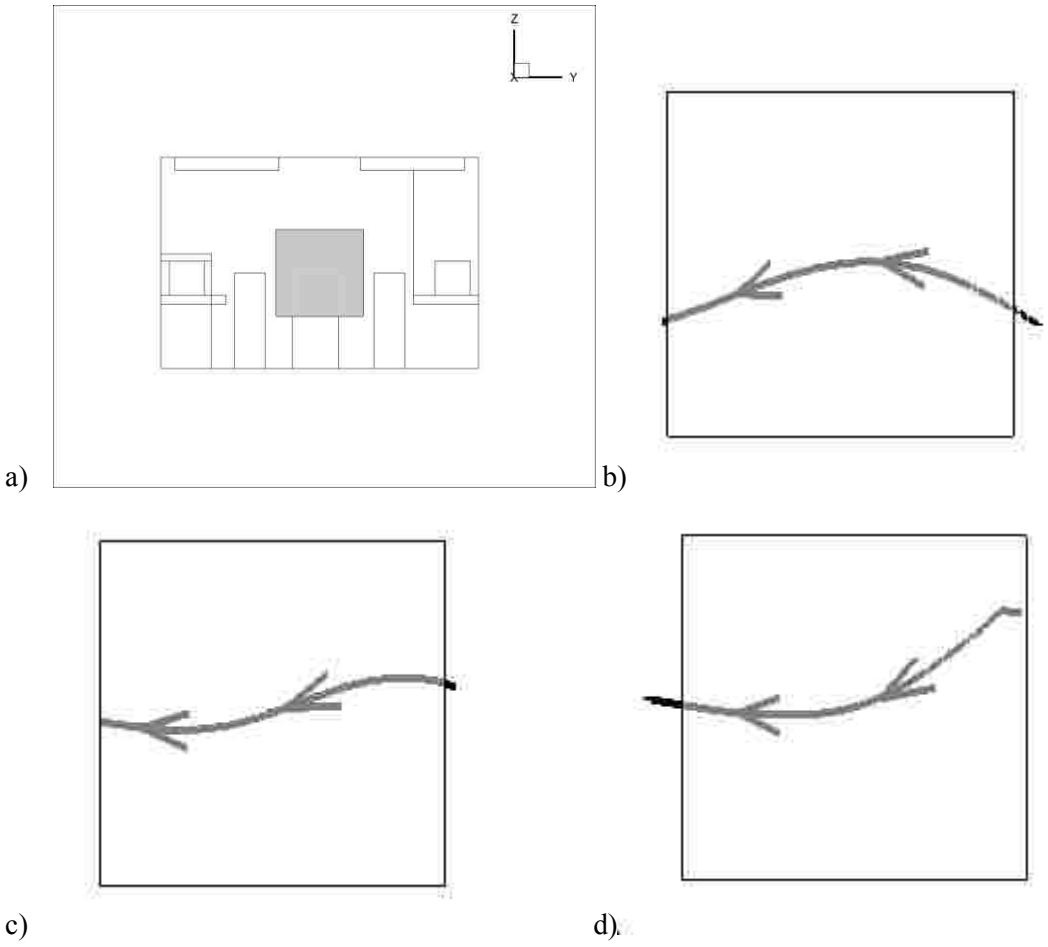

Figure D.3 ZY Plane view of an anomalous point on pole 4 – height of 1.1 m; a) location of stream trace, b) mesh N3, c) mesh N2, d) mesh N1

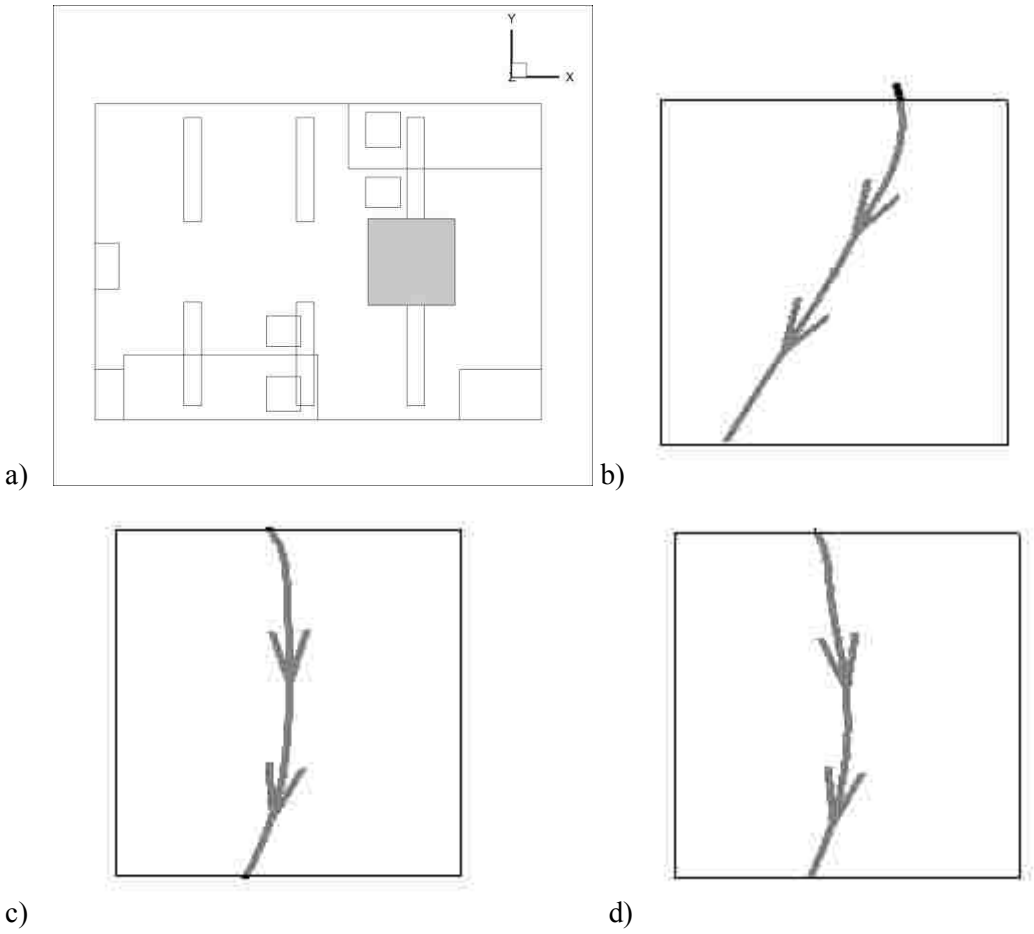

Figure D.4 XY Plane view of an anomalous point on pole 4 – height of 1.5 m; a) location of stream trace, b) mesh N3, c) mesh N2, d) mesh N1

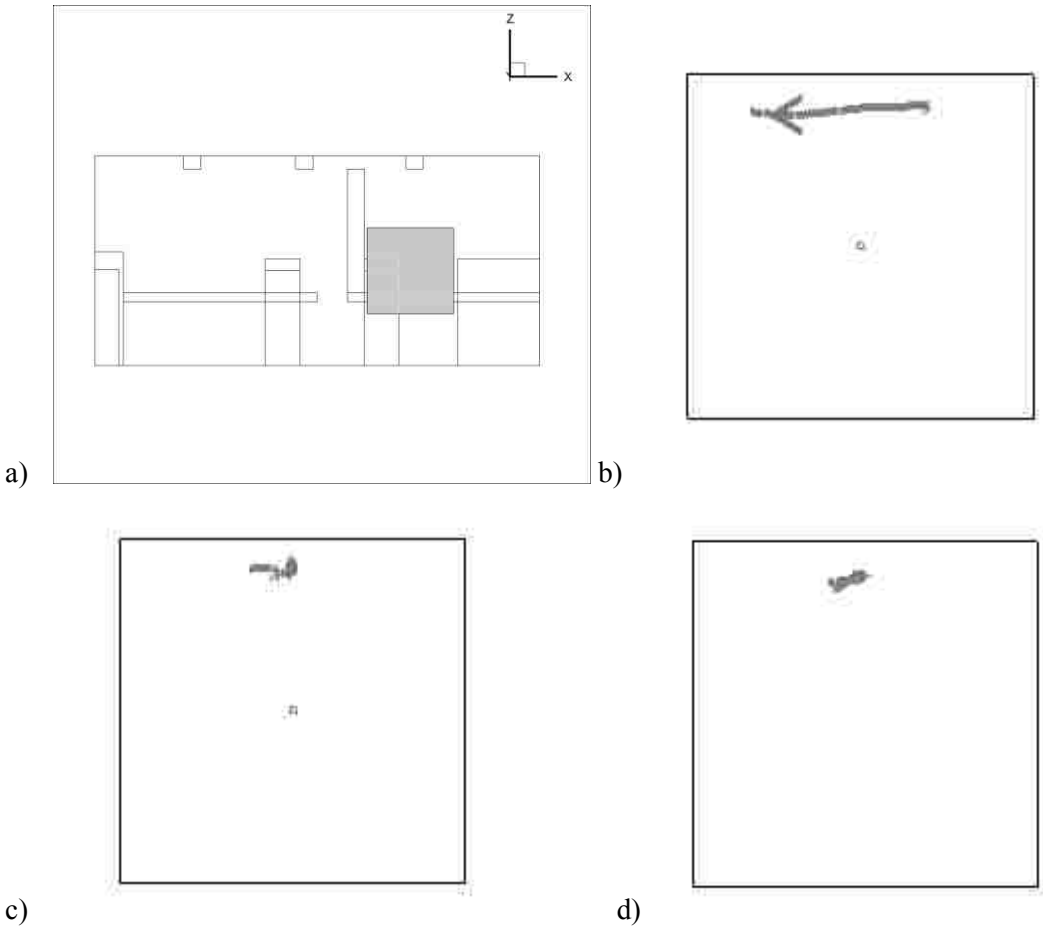

Figure D.5 ZX Plane view of an anomalous point on pole 4 – height of 1.5 m; a) location of stream trace, b) mesh N3, c) mesh N2, d) mesh N1

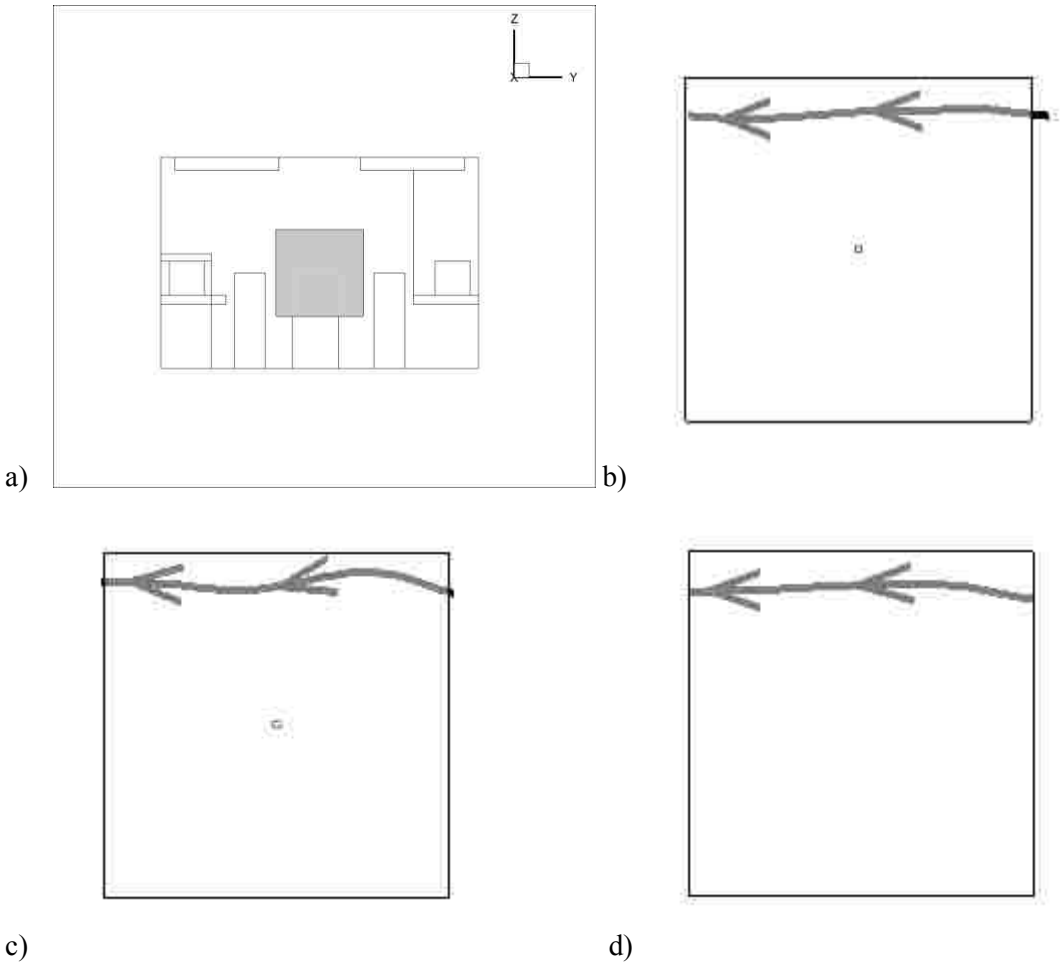

Figure D.6 ZY Plane view of an anomalous point on pole 4 – height of 1.5 m; a) location of stream trace, b) mesh N3, c) mesh N2, d) mesh N1

APPENDIX E

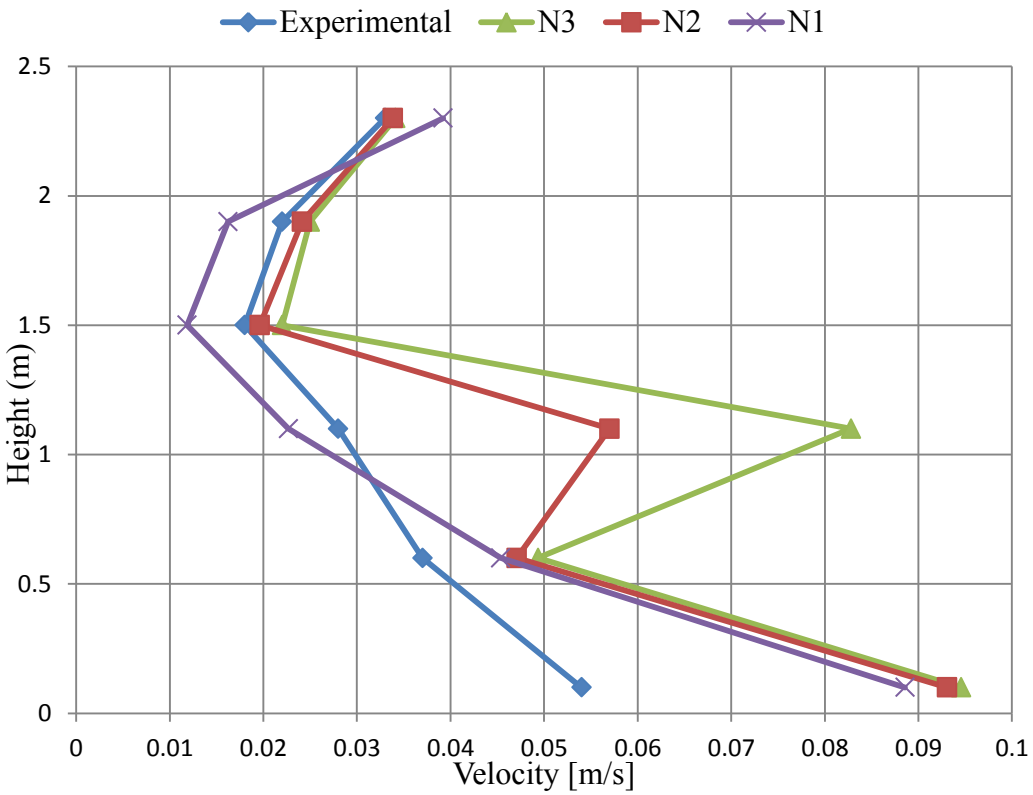

Figure E.1 - Experimental velocity vs. simulated velocity on pole 4 for N1, N2 & N3

VITA AUCTORIS

Aaron Alexander Aczel was born in 1983 in Windsor, Ontario, Canada. He completed secondary education at St. Joseph's Catholic High School in Windsor, Ontario in 2002. He then graduated from the University of Windsor with an Honours Bachelor Degree of Applied Science in Mechanical Engineering, Automotive Option, in 2006. Aaron joined the University of Windsor as a graduate student on a part-time basis in 2009. He is currently pursuing a Masters of Applied Science degree in Mechanical Engineering from the Department of Mechanical, Automotive and Materials Engineering with specialization in Computational Fluid Dynamics and Uncertainty Methods, expecting to graduate in October 2014.